Department of Applied Physics Aalto University School of Science

Transparent, conductive and flexible single-walled carbon nanotube films

Antti Kaskela

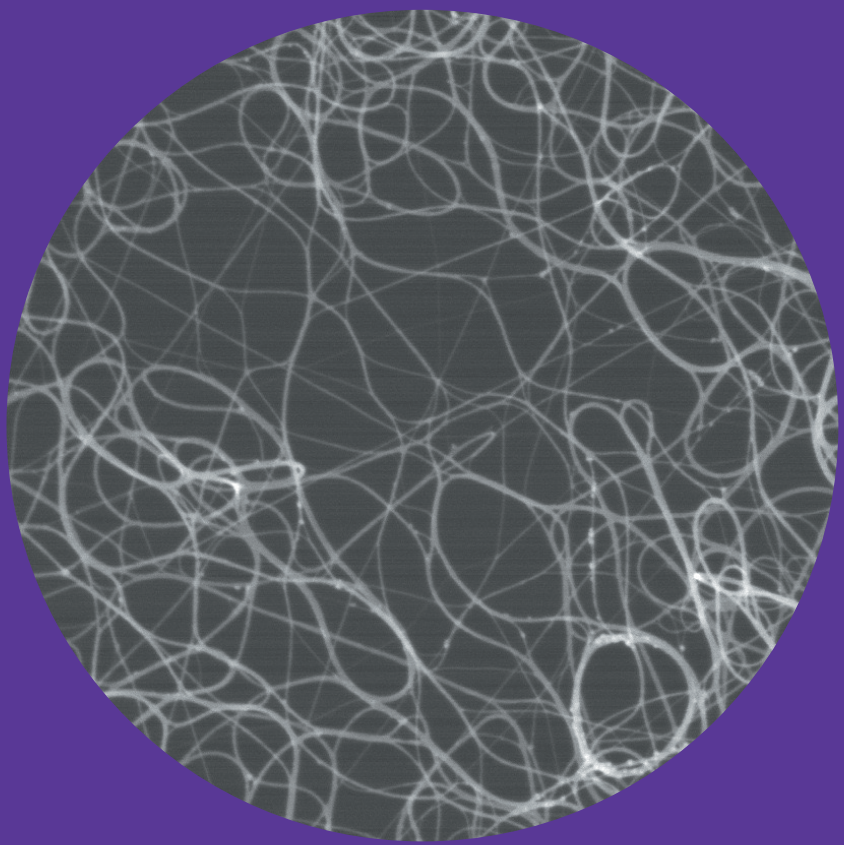

Aalto University

DOCTORAL DISSERTATIONS

Aalto University publication series
DOCTORAL DISSERTATIONS 197/2013

Transparent, conductive and flexible single-walled carbon nanotube films

Antti Kaskela

A doctoral dissertation completed for the degree of Doctor of Science (Technology) to be defended, with the permission of the Aalto University School of Science, at a public examination held at the lecture hall E of the school on 10 December 2013 at 12 o'clock.

Aalto University
School of Science
Department of Applied Physics
NanoMaterials Group

Supervising professor
Esko I. Kauppinen

Thesis advisor
Dr. Albert G. Nasibulin

Preliminary examiners
Prof. Taishi Takenobu, Waseda University, Japan
Dr. Stephan Hofmann, University of Cambridge, UK

Opponent
Prof. Shigeo Maruyama, Tokyo University, Japan

Aalto University publication series
DOCTORAL DISSERTATIONS 197/2013

ISBN 978-952-60-5458-2
ISBN 978-952-60-5459-9 (pdf)
ISSN-L 1799-4934
ISSN 1799-4934 (printed)
ISSN 1799-4942 (pdf)
http://urn.fi/URN:ISBN:978-952-60-5459-9

Unigrafia Oy
Helsinki 2013

Finland

441 697
Printed matter

Aalto University

Abstract

Aalto University, P.O. Box 11000, FI-00076 Aalto www.aalto.fi

Author
Antti Kaskela

Name of the doctoral dissertation
Transparent, conductive and flexible single-walled carbon nanotube films

Publisher School of Science

Unit Department of Applied Physics

Series Aalto University publication series DOCTORAL DISSERTATIONS 197/2013

Field of research Applied physics, Nanomaterials

Manuscript submitted 10 September 2013 **Date of the defence** 10 December 2013

Permission to publish granted (date) 29 October 2013 **Language** English

☐ **Monograph** ☒ **Article dissertation (summary + original articles)**

Abstract

Single-walled carbon nanotube (SWCNT) networks have a large application potential for future electronics as transparent conductive films. SWCNT networks (SWCNT-N) offer improved flexibility when compared to the current industry standard transparent conductive films (TCF), an example of which is indium tin oxide (ITO). SWCNTs can be synthesised from abundant raw materials, whereas indium supply is limited and has been a target of aggressive trade policies, thus increasing supply risks and price volatility. In order to make the SWCNT-Ns suitable for industrial applications, their performance must be made competitive with ITO and other TCF materials, whilst their manufacturing costs have to be minimised.

Understanding the performance limiting factors is important when it comes to the development of high performance SWCNT networks. The results presented here show that the bundle length has a major impact on the electrical performance of SWCNT networks. Optimisation of SWCNT growth conditions in aerosol-CVD reactors used for SWCNT synthesis led to an increase in SWCNT bundle length from 1.3 μm to 9.4 μm. Bundle diameter distributions were found to overlap, with mean bundle diameter measuring approximately 10 nm, and mean SWCNT diameters ranging from 1.4 to 1.7 nm. The increased bundle length led to a reduction in the number of the highly resistive bundle-bundle contacts and to improved performance. When the SWCNT-TCFs were chemically doped by nitric acid, sheet resistance was reduced down to 84 Ω/sq. at 90% transparency, thus making the SWCNT TCFs competitive with ITO on polymer films.

The intertube and interbundle contact resistances together with the effect of nitric acid treatment were studied by using conductive atomic force microscopy. The contact resistance values of pristine junctions were within the range of 29 kΩ - 532 kΩ for contacts between individual tubes and small bundles with less than 5 nm diameter. The contact resistance decreased with increasing tube or bundle diameter. Contact morphology had a major impact on the contact resistance values as X-contacts exhibited higher mean contact resistance of 180 kΩ, while the Y-contacts had mean contact resistance of 60 kΩ. When the contacts were exposed to strong nitric acid, the mean contact resistance was reduced by a factor of 3, although the length resistivity remained largely unchanged at around 8 kΩ/μm. The results indicate that the contact morphology and the diameter of contacting SWCNTs and bundles had a significant impact on the electrical transport across the contacts and that the nitric acid treatment mainly affected the network performance by modulating the contacts and reducing their contact resistances.

Furthermore, a novel room-temperature press transfer technique was developed. This dry, ambient temperature deposition method allowed for the rapid and direct deposition of variable thickness SWCNT networks to a wide range of substrates, from flexible polymers to glass, silicon and metals. The developed process eliminates harsh and detrimental purification and dispersion steps, thus maintaining the high intrinsic performance of SWCNTs. Fabrication of novel freestanding SWCNT networks was also demonstrated. The free-standing SWCNT networks can be used for a wide range of novel applications. The aerosol-CVD synthesised SWCNTs were also demonstrated as flexible counter-electrodes in dye-sensitised solar cells. The SWCNT-network was combined with electrochemically deposited PEDOT, reaching comparable performance with standard platinum catalyst with energy conversion efficiencies of up to 4%. Fabrication and properties of hybrid materials consisting of SWCNT networks coated with amorphous carbon deposited by low energy plasma were studied. The carbon coating improved the mechanical durability of SWCNT films under nanoindentation and scratching.

Keywords single-walled carbon nanotube, contact resistance, transparent conductive film, network, applications

ISBN (printed) 978-952-60-5458-2 **ISBN (pdf)** 978-952-60-5459-9

ISSN-L 1799-4934 **ISSN (printed)** 1799-4934 **ISSN (pdf)** 1799-4942

Location of publisher Helsinki **Location of printing** Helsinki **Year** 2013

Pages 101 **urn** http://urn.fi/URN:ISBN:978-952-60-5459-9

Aalto-yliopisto

Tiivistelmä

Aalto-yliopisto, PL 11000, 00076 Aalto www.aalto.fi

Tekijä
Antti Kaskela

Väitöskirjan nimi
Läpinäkyvät, johtavat ja joustavat yksiseinäiset hiilinanoputkikalvot

Julkaisija Perustieteiden korkeakoulu

Yksikkö Teknillisen fysiikan laitos

Sarja Aalto University publication series DOCTORAL DISSERTATIONS 197/2013

Tutkimusala Teknillinen fysiikka, nanomateriaalit

Käsikirjoituksen pvm 10.09.2013 **Väitöspäivä** 10.12.2013

Julkaisuluvan myöntämispäivä 29.10.2013 **Kieli** Englanti

☐ **Monografia** ☒ **Yhdistelmäväitöskirja (yhteenveto-osa + erillisartikkelit)**

Tiivistelmä

Yksiseinämäisillä hiilinanoputkilla on merkittävä sovelluspotentiaali tulevaisuuden elektroniikassa läpinäkyvinä johdemateriaaleina. Nanoputkiverkot ovat merkittävästi tällä hetkellä käytössä olevia läpinäkyviä johdemateriaaleja, kuten indium-tinaoksidia, taipuisampia. Hiilinanoputkiverkkoja voidaan valmistaa helposti saatavilla olevista raaka-aineista, kun taas hyödynnetyt indium-resurssit ovat voimakkaasti keskittyneet. Indium on myös ollut aggressiivisten vientirajoitusten kohteena, mikä on puolestaan lisännyt saatavuusriskiä ja aiheuttanut hinnanvaihteluita. Jotta hiilinanoputkiverkkoihin pohjautuvat materiaalit voivat kilpailla teollisissa sovelluksissa indium-tina-oksidin kanssa, niiden suorituskykyä on parannettava nykyisten kaupallisten materiaalien kanssa kilpailukykyiselle tasolle. Myös hiiliputkien valmistus- ja prosessointimenetelmiä on kehitettävä tuotantokustannusten madaltamiseksi.

Hiilinanoputkiverkkojen suorituskyvyn parantamiseksi on tärkeää ymmärtää suorituskykyä rajoittavia tekijöitä. Tämän väitöskirjan tulokset osoittavat, että hiilinanoputkien muodostamien kimppujen pituus on erittäin merkittävä verkkojen suorituskykyyn vaikuttava tekijä. Optimoimalla aerosolipohjaisen synteesireaktorin reaktio-olosuhteita, onnistuttiin hiilinanoputkien kimppujen pituutta kasvattamaan 1.3 μm:stä 9.4 μm:iin. Kimppujen halkaisijajakaumat olivat eri kasvatusolosuhteissa päällekkäisiä, keskihalkaisijan ollessa noin 10 nm. Yksittäisten hiilinanoputkien keskimääräiset halkaisijat olivat tyypillisesti 1.4 to 1.7 nm välillä. Pidempi kimppupituus vähentää korkean vastuksen kimppu-kimppu-liitosten lukumäärää ja pienentää näin verkon kokonaisvastusta. Typpihappokäsittelyn avulla verkon pintavastus onnistuttiin pienentämään arvoon 84 Ω/neliö 90 % valonläpäisyllä, tehden verkoista suorituskyvyltään kilpailukykyisiä polymeerikalvoille kasvatetun indium-tina-oksidin kanssa.

Putkien ja kimppujen välisien kontaktien liitosvastuksia, niiden pituusvastuksia sekä typpihappokäsittelyn vaikutusmekanismia tutkittiin johtavan atomivoimamikroskopian avulla. Käsittelemättömien liitoksien liitosvastukset vaihtelivat 29 kΩ ja 532 kΩ välillä, pääosin yksittäisistä nanoputkista ja halkaisijaltaan pienistä, alle 5 nm kimpuista, koostuvalle näytepopulaatiolle. Liitosvastuksen havaittiin pienenevän kasvavan putki- ja kimppuhalkaisijan mukana. Liitoksen geometrialla havaittiin olevan merkittävä vaikutus liitosvastukseen. X-tyyppisien liitoksien kontaktivastus oli keskimäärin 180 kΩ, kun Y-tyyppisten liitoksen keskimääräinen kontaktivastus oli 60 kΩ. Kun X-tyyppisiä liitoksia käsiteltiin typpihapolla, kontaktivastus pieneni tekijällä 3, kun taas pituusvastus pysyi lähes vakiona noin 8 kΩ/μm tasolla. Tulosten mukaan typpihappokäsittely parantaa verkon suorituskykyä lähinnä pienentämällä liitosvastuksia.

Lisäksi tässä väitöskirjassa tutkittiin useita hiilinanoputkiverkkojen sovellusalueita ja valmistettiin uudenlaisia itsekantavia nanoputkiverkkoja. Työssä kehitettiin uusi, huoneenlämpötilassa toimiva valmistusmenetelmä hiiliputkiverkkojen siirtämiseen keräyssuodattimelta sovelluksissa tarvittaville pohjamateriaaleille. Menetelmän osoitettiin mahdollistavan eri paksuuksien hiilinanoputkiverkkojen nopean ja suoraviivaisen siirron laajalle joukolle alustamateriaaleja, mukaan lukien joustavat polymeerit, lasi, pii sekä metallikalvot. Menetelmän merkittävänä etuna on, että sen kanssa ei tarvita haitallisia ja aikaa vieviä puhdistus- ja dispersointikäsittelyjä ja tämä mahdollistaa hiiliputkien korkean johtavuuden hyödyntämisen. Hiilinanoputkiverkkoja käytettiin lisäksi myös joustavina väriaineherkistetyn aurinkokennon vastaelektrodimateriaalina. Yhdistämällä hiilinanoputkiverkko elektropolymerisoidun PEDOT-polymeerin kanssa saavutettiin platinakatalyyttiä vastaava suorituskyky, parhaimmillaan 4 % hyötysuhteella. Viimeisenä aihealueena tutkittiin hiilinanoputkien ja amorfisten plasmakasvatuksella valmistettujen hiilipinnoitteiden yhdistämistä hybridirakenteeksi. Hiilipinnoitteen käyttö paransi merkittävästi hiilinanoputkiverkon mekaanista kestävyyttä, hybridimateriaalin pysyessä johtavana ja läpinäkyvänä.

Avainsanat yksiseinäinen hiilinanoputki, liitosvastus, läpinäkyvä johdekalvo, verkko, sovellukset

ISBN (painettu) 978-952-60-5458-2 **ISBN (pdf)** 978-952-60-5459-9

ISSN-L 1799-4934 **ISSN (painettu)** 1799-4934 **ISSN (pdf)** 1799-4942

Julkaisupaikka Helsinki **Painopaikka** Helsinki **Vuosi** 2013

Sivumäärä 101 **urn** http://urn.fi/URN:ISBN:978-952-60-5459-9

Preface

This research was conducted between the spring of 2008 and the spring of 2013 in the Nanomaterials Group at the Department of Applied Physics of Aalto University's School of Science. I have been privileged to work with leading experts in the field in a research group with excellent resources and equipment. During this time I have learned a great deal, and been presented with fantastic opportunities to build a wide range of capabilities and skills while working with multiple academic and industrial partners.

Several people have contributed significantly to this work and I would like to use this opportunity to acknowledge them. First, professor Esko I. Kauppinen, my thesis supervisor, has been absolutely instrumental in the successful completion of this work. He has been an excellent supervisor and mentor, and has always been able to see the big picture and drive the research towards its important goals. He has also been very flexible, giving a plenty of room for young scientists to work independently. Dr. Albert Nasibulin, the thesis instructor, has taught me a lot and made a major contribution to this work. I would like to thank him for teaching me many of the experimental skills related to aerosol synthesis of SWCNTs, fabrication of networks and also for taking the time to teach me how to write academic manuscripts. Albert has also been keen to find applications for the developed materials and techniques, thus helping to demonstrate the important engineering aspects of the research.

Dr. David P. Brown and Mr. Brad Aitchison from Canatu Ltd. were important collaborators in the work leading to the development of pilot scale synthesis reactors. Getting to work closely with an industrial partner was a unique opportunity for such an early phase of my career. Dr. Abdou Hassanien and Dr. Andrej Znidarsic contributed significantly with their C-AFM expertise to understanding the nanoscale behaviour of the SWCNT networks and to understanding the role of chemical treatment. The thesis became much more convincing with the results of this fruitful collaboration and I am deeply appreciative of the contribution made by both of them. Dr. Janne Halme and Dr. Kerttu Aitola from New Energy Technologies group of Aalto also contributed to this thesis during extensive collaboration related to the utilisation of SWCNT networks as electrodes in dye-sensitised solar cells, carrying out experiments and characterisation. They should be thanked for their work. Professor Jari Koskinen initiated the research of PVD-carbon coating of the SWCNT networks. He has been a pleasure to work with and I am very happy that the collaboration continues as a joint research project. Professor Yutaka Ohno from Nagoya University has also contributed to this work and I would also like to thank him for hosting me during the research visits to his labs.

I would like to acknowledge a few other colleagues from Nanomaterials Group, all of whom have also contributed to this work: Dr. Toma Susi, Mr. Patrik Laiho, Dr. Hua Jiang, Dr. Ying Tian, Mr. Kimmo Mustonen and Dr. Marina Timmermans. You have been nice colleagues and a pleasure to work with. Mrs. Marita Halme deserves to be thanked for helping with all the practicalities and bureaucracy. I would also like to thank the pre-examiners of this thesis, professor Taishi Takenobu and Dr. Stephan Hofmann who helped to improve the text with their comments. I am also thankful to professor Shigeo Maruyama, for accepting the invitation to serve as the opponent. This research has been made possible with funding from multiple sources, including TEKES, Academy of Finland, Aalto University's MIDE and AEF-programs via CNB-E and MOPPI-projects and National Graduate School in Nanoscience. The electron microscopes at the National Nanomicroscopy Center at Aalto University were used for this work and were much appreciated.

Finally, I would like to thank my wife Suvi for her love, support and everything else. Having you on my side during the years spent with this thesis has had a huge impact on this work.

In Espoo
11.11.2013

Antti Kaskela

Contents

List of Publications

The thesis consists of a summary and the following original publications. The publications were selected based on the author's own contribution from those which were accepted for publication by early-2013, when writing of the thesis commenced.

I Kaskela, A., Nasibulin, A.G., Zavodchikova, M., Aitchison, B., Papadimitratos, A., Tian, Y., Zhu, Z., Jiang, H., Brown, D.P., Zakhidov, A., and Kauppinen, E.I., Aerosol synthesized SWCNT networks with tuneable conductivity and transparency by dry transfer technique, Nano Letters 10, 4349-4355 (2010).

II Nasibulin, A. G., Kaskela, A., Mustonen, K., Anisimov, A. S., Ruiz, V., Kivistö, S., Rackauskas, S., Timmermans, M. Y., Pudas, M., Aitchison, B., Kauppinen, M., Brown, D. P., Okhotnikov, O. G., and Kauppinen, E. I., Multifunctional freestanding single-walled carbon nanotube films, ACS Nano 5, 3214-3221 (2011).

III Znidarsic, A., Kaskela, A., Laiho, P., Gaberscek, M., Ohno, Y., Nasibulin, A. G., Kauppinen, E. I., and Hassanien, A., Spatially Resolved Transport Properties of Pristine and Doped Single-Walled Carbon Nanotube Networks," Journal of Physical Chemistry C 117, 13324–13330 (2013).

IV Aitola, K., Borghei, M., Kaskela, A., Kemppainen, E., Nasibulin, A.G., Kauppinen, E.I., Lund, P.D., Ruiz, V., and Halme, J., Flexible metal-free counter electrode for dye solar cells based on conductive polymer and carbon nanotubes, Journal of Electroanalytical Chemistry 683, 70-74 (2012).

V Kaskela, A., Koskinen J., Jiang, H., Tian, Y., Liu X., Susi, T., Kaukonen, M., Nasibulin, A.G., and Kauppinen E.I., Improvement of the mechanical properties of single-walled carbon nanotube networks by carbon plasma coatings, Carbon 53, 50–56 (2013).

Author's Contribution

I: Author contributed to all parts of this work, conducted out the majority of the experiments, synthesised the SWCNT materials and was responsible for writing the manuscript.

II: Author contributed to SWCNT synthesis, sample preparation and experiments and co-wrote the manuscript.

III: Author contributed to experimental design, sample fabrication and characterisation, data analysis and co-wrote the manuscript.

IV: Author contributed to experimental design, synthesised and processed the counter electrodes, carried out SWCNT material characterisation and contributed to the writing of the manuscript.

V: Author contributed to material synthesis, PVD-coatings, characterisation and wrote the manuscript.

Other Featured Publications

I. Heras, A., Colina, A., Lopez-Palacios, J., Kaskela, A., Nasibulin, A.G., Ruiz, V., Kauppinen, E.I., Flexible optically transparent single-walled carbon nanotube electrodes for UV-Vis absorption spectroelectrochemistry, Electrochemistry Communications 11, 442-445 (2009).

II. Kivistö, S., Hakulinen, T., Kaskela, A., Aitchison, B., Brown, D.P., Nasibulin, A.G., Kauppinen, E.I., Härkönen, A., and Okhotnikov, O.G., Carbon nanotube films for ultrafast broadband technology, Optics Express 17, 2358-2363 (2009).

III. Aitola, K., Kaskela, A., Halme, J., Ruiz, V., Nasibulin, A.G., Kauppinen, E.I., and Lund, P.D., Single-Walled Carbon Nanotube Thin-Film Counter Electrodes for Indium Tin Oxide-Free Plastic Dye Solar Cells, Journal of the Electrochemical Society 157, pp. B1831-B1837 (2010).

IV. Aitola, K., Halme, J., Halonen, N., Kaskela, A., Toivola, M., Nasibulin, A.G., Kordás, K., Tóth, G., Kauppinen, E.I., and Lund, P.D., Comparison of dye solar cell counter electrodes based on different carbon nanostructures, Thin Solid Films 519, 8125-8134 (2011).

V. He, M., Chernov, A., Obraztsova, E., Sainio, J., Rikkinen, E., Jiang, H., Zhu, Z., Kaskela, A., Nasibulin, A., Kauppinen, E., Niemelä, M., and Krause, O., Low temperature growth of SWNTs on a nickel catalyst by thermal chemical vapor deposition, Nano Research 4, 334-342 (2011).

VI. Susi, T., Kaskela, A., Zhu, Z., Ayala, P., Arenal, R., Tian, Y., Laiho, P., Mali, J., Nasibulin, A. G., Jiang, H., Lanzani, G., Stephan, O., Laasonen, K., Pichler, T., Loiseau, A., and Kauppinen, E. I., Nitrogen-Doped Single-Walled Carbon Nanotube Thin Films Exhibiting Anomalous Sheet Resistances, Chemistry of Materials 23, 2201-2208 (2011).

VII. Laiho, P., Susi, T., Kaskela, A., Nasibulin, A. G., Kauppinen, E. I., Optoelectronic performance of nitrogen-doped SWCNT films, Journal of Nanoelectronics and Optoelectronics 7, 68-72 (2012).

VIII. Mikheev, G. M., Nasibulin, A. G., Zonov, R. G., A. G., Kaskela, A., Kauppinen, E. I., Photon-drag effect in single-walled carbon nanotube films, Nano Letters 12, 77-83 (2012).

IX. Mustonen, K., Susi, T., Kaskela, A., Laiho, P., Tian, Y., Nasibulin, A.G., Kauppinen, E.I., Influence of single-walled carbon nanotube bundle diameters on dry-deposited thin film optoelectronic performance, Beilstein Journal of Nanotechnology No. 3, 692-702 (2012).

X. D.-M. Sun, M. Y. Timmermans, A. Kaskela, A. G. Nasibulin, S. Kishimoto, T. Mizutani, E. I. Kauppinen, and Y. Ohno, “Mouldable all-carbon integrated circuits,” Nature Communications 4, 1–8, (2013).

List of Symbols and Abbreviations

a	Extinction coefficient
AFM	Atomic force microscopy
C-AFM	Conductive atomic force microscopy
CVD	Chemical vapour deposition
DLC	Diamond-like carbon
FTO	Fluorine doped indium tin oxide
FSF	Free standing film
HNO_3	Nitric acid
ITO	Indium tin oxide
L	Length
MWCNT	Multi-walled carbon nanotubes
PVD	Physical vapour deposition
R	Resistance
R_s	Sheet resistance
SBS	Sodium dodecylbenzenesulfonate
SDS	Sodium dodecyl sulphate
SEM	Scanning electron microscopy
$SOCl_2$	Thionyl chloride
SPM	Scanning probe microscopy
SWCNT	Single-walled carbon nanotube
T	Transmittance
TCF	Transparent conducting film
TEM	Transmission electron microscopy

1 Introduction

Single-walled carbon nanotubes (SWCNT) have a wide application potential for future electronics due to their unique physical and chemical properties [1]. The properties of SWCNTs are determined by their chirality whilst their band structure can be metallic, semi-metallic or semi-conductive. Random SWCNT networks (SWCNT-N) have been suggested as a potential route to the early utilisation of SWCNTs in applications such as transparent conductive films (TCF) [2], while challenges with manipulation, control and accurate positioning of individual SWCNTs still limit the use of individual SWCNTs, despite recent developments [3].

TCFs are an interesting application area due to their importance for several electronics applications, such as flat panel displays, touch sensors and photovoltaics [4], [5], [2]. The industry standard TCF material, ITO (90% In / 10% Sn), offers a good optoelectrical performance, reasonable environmental stability and good etchability, although it also has several drawbacks such as limited flexibility and limited performance on thermally sensitive substrates, a high refractive index and high material and processing costs (600 USD/kg, 2013) [6], [7]. The majority of the global indium supply is controlled by China and has been a target of aggressive trade policies, leading to global price fluctuations and higher supply risks [8].

SWCNT networks and graphene have been suggested as potential replacements for ITO, as they provide improved flexibility, higher maximum transparency at visible wavelengths and improved refractive index matching [2], [1]. For the industrial adaptation of these alternative materials it is essential that their optoelectrical performance is improved to a level which matches or beats ITO and other competing TCF materials, and that their manufacturing cost is minimised. New device designs using the unique properties of SWCNT-TCFs should be developed to improve the value proposition of the alternative materials. The benefits should be sufficiently large to justify the switching costs of adapting the new materials and technology. The thesis aims to contribute towards these goals and is organised around two research questions:

1) What determines the overall performance of a SWCNT-TCFs? How does the morphology of the SWCNT network and chemical treatment affect the performance?

2) What kind of applications are the SWCNT-TCFs suitable for and how can the SWCNT networks be processed and modified?

The SWCNTs used in this thesis were synthesised with an aerosol-CVD process, based on catalytic decomposition of carbon monoxide (CO) on iron nanoparticles. The aerosol-CVD process produces clean and high quality SWCNTs, thus eliminating the need for additional cleaning steps. The synthesis process was optimised to improve the electrical performance of SWCNT-TCFs. The improved performance was found to be linked to increased SWCNT bundle length, which in turn led to reduced number of resistive bundle-bundle contacts in SWCNT-Ns. As a result, SWCNT-TCFs with low temperature ITO on polymer comparable optoelectrical performance of 110 Ω/sq. at 90% (Publication 1) and 84 Ω/sq. at 90% (Publication 2) were demonstrated. Contact resistance

characteristics and the effects of chemical treatment were studied for the first time on surfactant free samples with conductive-AFM (Publication 3). The results showed that SWCNT contact resistance was reduced with increased bundle diameter and by acid treatment, while the resistance along the SWCNT remained largely unchanged despite the chemical treatment.

A rapid room temperature press transfer method was developed to deposit the SWCNT-Ns on a wide range of substrates including flexible polymers, glasses, metals, silicon etc. This novel deposition method simplifies the device fabrication and helps to eliminate the harsh and detrimental chemical purification and dispersion processes used with other deposition methods. The press-transfer can be combined with liquid densification and acid treatments, which can further improve the optoelectrical performance. Furthermore, the transfer method was used for fabrication of novel freestanding SWCNT-TCFs, with tuneable thickness, transparency and sheet resistance. Several applications of SWCNT-Ns were demonstrated, including capacitive touch sensors and dye sensitised solar cells with SWCNT-Ns as flexible, platinum free counter electrode material (Publication 4). In addition, improvement of mechanical properties of SWCNT-networks with carbon coatings was studied, demonstrating hybrid materials with improved mechanical durability under nanoindentation and scratching (Publication 5).

The thesis is organised into six chapters. The introduction motivates the study and summarises the main findings. The theoretical background is given in the second chapter; the third chapter compares the optoelectrical performance of various TCF materials. The experimental methods are presented in the next chapter. In the fifth chapter the main results are presented and discussed whilst the final chapter summarises the conclusions and plans for future work. The original publications are reprinted as appendices.

2 Theory

2.1 Carbon Nanotubes

Carbon nanotubes belong to a diverse carbon nanostructure family and can be represented as a cylindrically rolled graphene sheet with a high aspect ratio. Graphene is a hexagonally arranged, 2-dimensional carbon crystal. The electronic and optical properties of SWCNTs are dependent on their chiral configuration and 1-dimensional confinement. CNTs are classified as either single-walled carbon nanotubes (SWCNT) or multi-walled carbon nanotubes (MWCNT), based on the number of concentric carbon shells. Carbon nanotubes are closely related to other important classes carbon nanostructures: graphene and fullerenes.

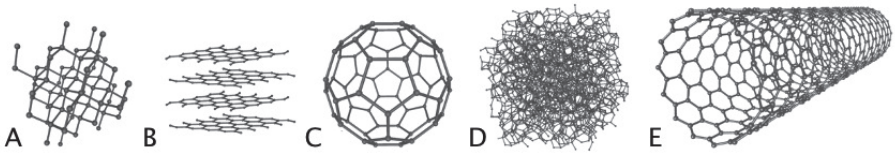

Figure 2.1. A few different allotropes of carbon, a) diamond lattice consisting of sp_3 bonded carbon atoms, b) graphite, which consists of vertically stacked graphene sheets, c) C60 fullerene, d) amorphous carbon and e) a single-walled carbon nanotube (adapted from Wikimedia Commons under CC Attribution-Share Alike 3.0 Unported License [9]).

CNTs have received a great deal of research interest since the hallmark publication reporting multi-walled carbon nanotubes by Sumio Iijima [10]. Soon single-walled carbon nanotubes (SWCNTs) were initially observed and reported by Iijima and Ichihashi and independently by Bethune and collaborators in 1993 [10], [11]. More recent times have seen the emergence of graphene and it has further attracted interest due to its flat, 2d-structure and unique electronic properties [12].

The SWCNT structure can be defined by using the (n, m)-notation (Figure 2.1.2). This can be done by using the graphene unit cell base vectors $\overline{a_1}$ and $\overline{a_2}$ defining the chiral vector $\overline{C_h}$, which connects the two equivalent points, which are joined when the graphene ribbon is conceptually rolled to a tubular SWCNT structure as

$$\overline{C_h} = n\overline{a_1} + m\overline{a_2}, \qquad (2.1.1)$$

a specific carbon nanotube structure is uniquely determined by (n, m) indices (n, m = 1, 2, ..., n ≥ m).

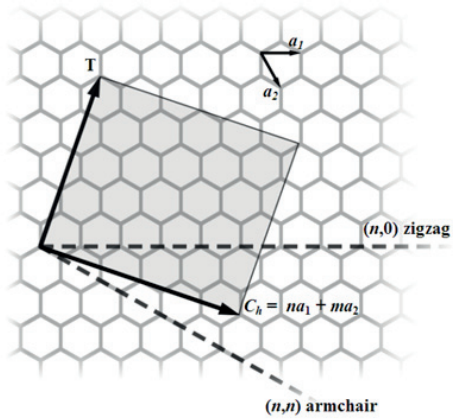

Figure 2.2. The flat graphene sheet, which is used as the basis for SWCNT-type classification. The chiral vector, $\overline{C_h}$, is defined by the graphene unit cell vectors a_1 and a_2 whilst the type of the SWCNT is described by (n, m)-index pair (adapted from Wikimedia Commons as public domain [13]).

When n = m, the SWCNT is classified as armchair. The armchair tubes have a metallic electron structure, with zero band-gap. For the armchair tubes the chiral angle reaches its maximum at 300. The name arises from the armchair-resembling structure of the carbon atoms in a direction perpendicular to the tube axis (Figure 2.3). In the other limiting case m = 0 with a chiral angle of 0° and the nanotube is of "zigzag" type. All of the other nanotube types between these limiting cases are classified as "chiral" nanotubes.

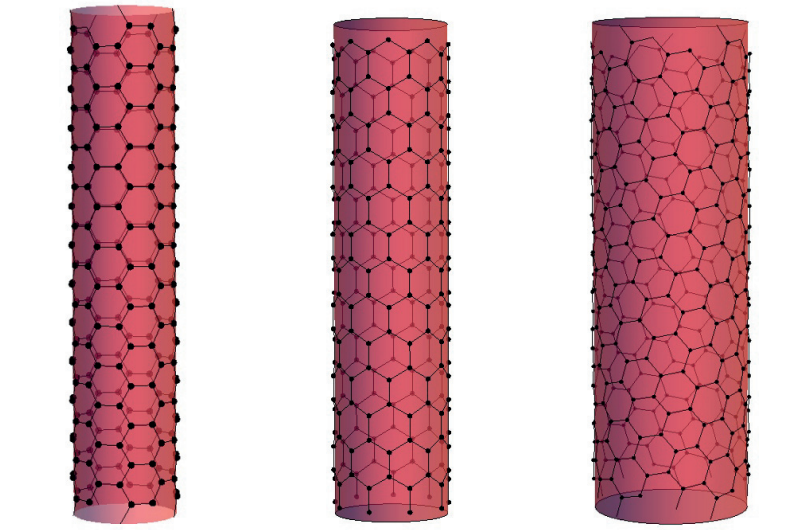

Figure 2.3. Armchair (n = m) and zigzag (m = 0) are the two limiting nanotube categories at chiral angles of 30° and 0°. All the other carbon nanotube types which fall between these limiting cases are classified as chiral nanotubes.

2.2 SWCNT Synthesis

SWCNT synthesis methods can be divided into physical or chemical processes. The physical processes rely on vaporisation of a graphite target which also contains catalyst metal, typically with an electrical arc or by pulsed laser beam [11], [14], [15]. Vaporised carbon condenses and dissolves in to metal catalyst particles, thus leading to the formation of crystalline SWCNTs. The high carbon concentration leads to the formation of undesired byproducts, such as MWCNTs, carbon soot, which are mixed with the SWCNTs. Extensive purification and separation treatments are required to isolate the SWCNTs [16].

The chemical processes are based on the catalytic decomposition of carbon containing precursors, which are delivered to the process in the gas phase. They can be tuned to produce selectively single-walled, double-walled or multi-walled tubes by altering the gas atmosphere or by modifying the catalyst particle composition and size [17], [18]. Traditionally, CVD-synthesis has relied on substrate supported catalyst particles. In the case of substrate supported CVD, the SWCNTs are grown on the substrate and can be used in some applications without additional processing. However, selection of the substrates is limited to materials which withstand the elevated temperatures required for the SWCNT growth [22]. The catalyst particles can also be brought to the synthesis reactor as aerosol in High Pressure Carbon Monoxide (HIPCO) and floating catalyst chemical vapour deposition processes (aerosol-CVD) [19], [20], [21].

Most synthesis methods produce SWCNTs mixed with impurities such as amorphous carbon and residual catalyst particles. Indeed, the impurities often have to be removed before the carbon nanotubes can be used for applications. Unfortunately, the harsh cleaning procedures are time consuming and detrimental to the performance of the carbon nanomaterials [23], [24], [25], [26].

2.3 Electronic Properties

The electrical properties of SWCNTs are dependent on their structure and can be metallic, semi-metallic or semi-conductive with a band-gap of approximately 0.7 eV / d (nm). The tubes which fulfil the criterion n = m, have metallic band structure. In contrast, in terms of the tubes for which n - m = 3 * z, there are states at the corners of the first Brillouin zone and the tubes are semi-metallic with a small, curvature induced band-gap of order of 100 meV. These tubes exhibit metallic behaviour at room temperature due to thermal activation [27]. The SWCNTs for which n - m ≠ 3 * z, are semi-conductive and exhibit diameter dependent band-gap (Here n, m, z = 1, 2, 3,...).

The band structure of carbon nanotubes can be described with a simple tight binding model of graphene, where the valence and conduction bands touch at the corner points of the first Brillouin zone, leading to semi-metallic behaviour with zero band-gap. The electron energy is given by

$$E_{2D}(k_x k_y) = \pm\gamma_0 \left[1 + 4\cos(\frac{\sqrt{3}k_x a}{2})\cos(\frac{k_y a}{2}) + 4\cos^2(\frac{k_y a}{2}) \right], \qquad (2.1)$$

where k_x, and k_y are the wave-vectors, γ_o is the nearest neighbour transfer integral and a = 0.246 nm is the in-plane lattice constant. Now, for the SWCNTs the electrons are 1D confined and the allowed states are parallel lines in the reciprocal space. The cross-sectional sub-bands, which are sliced from the dispersion cone of graphene's are shown in Figure 2.4. The dispersion relation of a i^{th} sub-band is given by the following relation,

$$E_i(k) = \pm\left(\left(\frac{h}{2\pi}v_F k\right)^2 + \left(\frac{E_i^g}{2}\right)^2\right)^{1/2}, \qquad (2.2)$$

where E and k are the distances from the centre point of graphene's dispersion cone in units of energy and wave-vector, v_F is the Fermi-velocity (approximately $8*10^5$ m/s) and the $E^g{}_i$ is the i^{th} energy gap. Furthermore, the SWCNT density of states exhibits the one-dimensional system characteristic van Hove singularities.

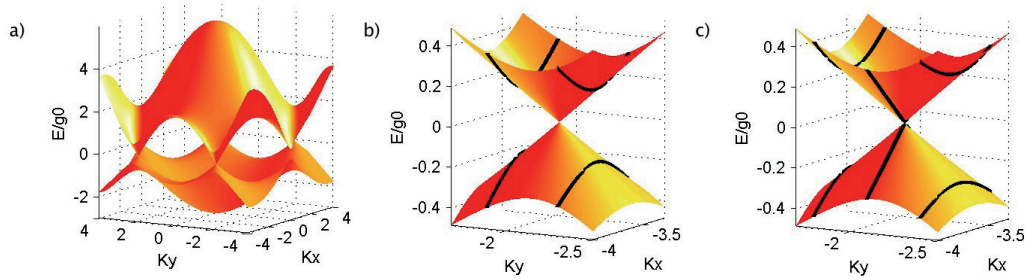

Figure 2.4. a) The band structure of SWCNTs can be described by using the graphene dispersion relation. b) The semi-conducting SWCNTs have a diameter dependent band-gap as indicated by the black lines. c) The metallic tube band structure (adapted from Wikimedia Commons as public domain [28]).

2.4 Optical Properties

Optical absorption spectroscopy relies on determination of the attenuation of light passing through a sample as a function of incident wavelength. The optical losses are linked to the sample thickness by the Beer-Lambert's law,

$$I(L) = I_0 e^{-aLc} \qquad (2.3)$$

where I_o is the incoming light intensity, L is the optical path length, a is the wavelength dependent extinction coefficient and c is the concentration of the absorbing species. For nanotube characterisation, the relevant wavelength typically ranges from 200 nm up to 2600 nm. The typical SWCNT absorption spectrum contains multiple characteristic peaks. First, the metallic tubes contribute to M_{11} transition, which originates from transitions between the edges of the joint density of states of the metallic SWCNT. The semi-conducting tubes generate two distinct peaks, namely E_{11} and E_{22}, which correspond to the two lowest transitions between the van Hove singularities [29]. The optical absorption spectra can be used for SWCNT diameter distribution estimation [30]. In typical samples which contain a mixture of SWCNTs, all the transitions are visible and the peaks are significantly broadened. For the characterisation of the optoelectrical performance of SWCNT TCFs, transmittance at 550 nm wavelength is typically used [31].

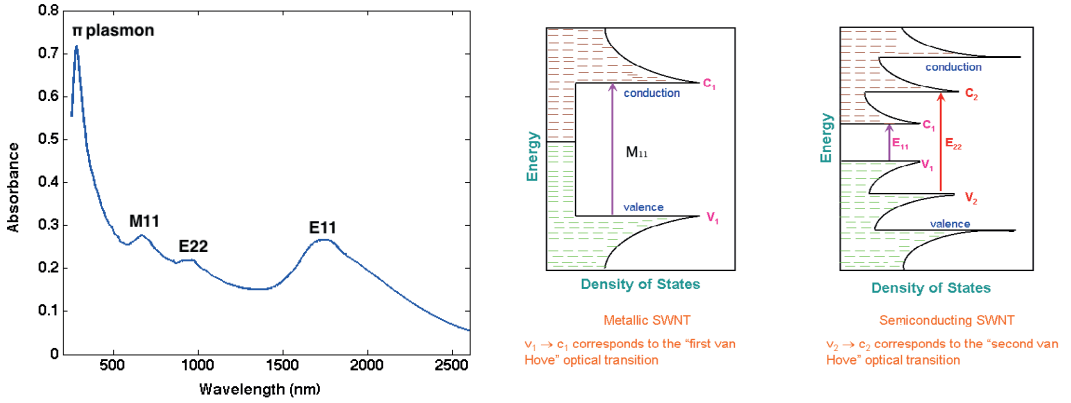

Figure 2.5. The typical absorption spectrum of a SWCNT sample and the related optical transitions (transitions adapted from Wikimedia Commons under CC Attribution-Share Alike 3.0 Unported License [32])

Raman-spectroscopy is another widely used technique for the characterisation of SWCNTs. It is based on the inelastic scattering of photons due to the interaction between the optical field and the optical phonons [33]. It can be used for estimation of SWCNT diameter, band-structure and the number of defects. Due to the resonant nature of this technique, only the tubes whose band-gap is in resonance with the excitation laser wavelength are active, thus meaning that the complete Raman-characterisation of a SWCNT sample requires a multi-source or a tuneable laser system [34].

2.5 SWCNT Networks

Carbon nanotube networks are a straightforward path for utilisation of the SWCNTs. The networks consist of a large number of different nanotubes and nanotube bundles and their aggregate properties determine the network performance. Therefore, the degree of required control is reduced and networks are seen as a likely short term route to SWCNT applications. As most of the synthesis processes produce approximately 2/3 of semi-conducting and 1/3 of metallic tubes, there are distinct behaviour regions of SWCNT networks as function of network density, as schematically depicted in Figure 2.6. In low density networks there are no percolating paths through the network and therefore no conduction. When the SWCNT density is increased above the percolation limit initially there are no metallic percolating paths due to the higher fraction of semi-conducting tubes and the network devices exhibit semi-conductive behaviour, meaning they can be used as thin-film transistor channel material [35]. When the network density is further increased, the metallic tubes eventually reach the percolation limit. The network starts to exhibit metallic behaviour with ohmic current-voltage characteristics. This thesis focusses on metallic SWCNT networks which are relevant for TCF applications.

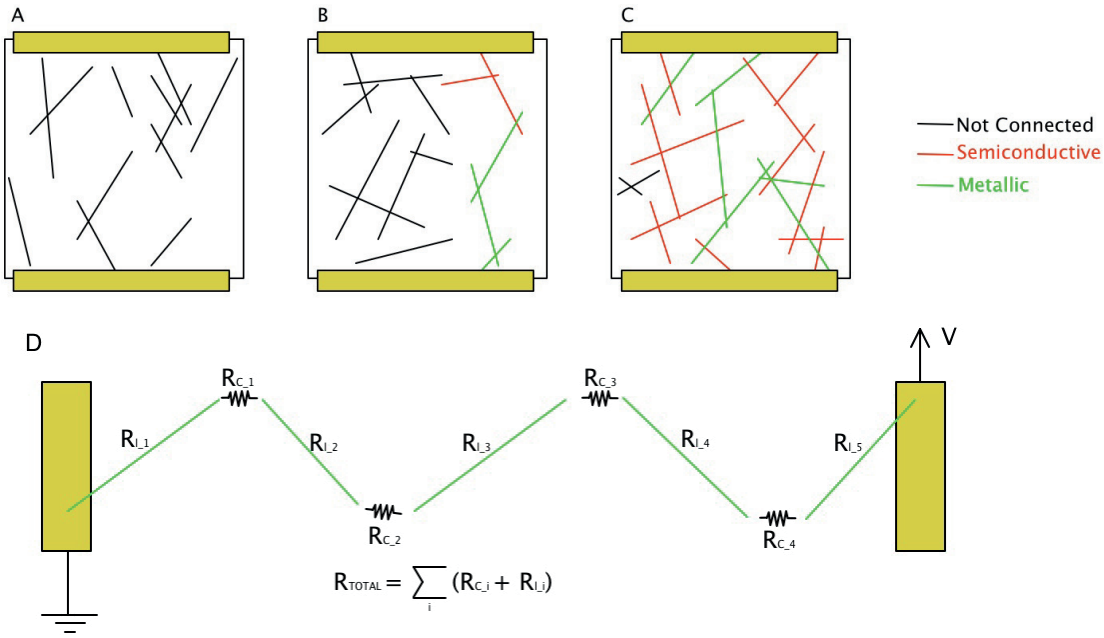

Figure 2.6. The network morphology and transport properties of SWCNT-Ns are closely linked. a) At the low density limit, the SWCNTs do not form a percolating path between the top and bottom electrodes (yellow). b) When the density increases, percolating paths, including semi-conductive tubes (red) are formed, thus leading to semi-conductive transport and c) at high SWCNT densities metallic SWCNTs form percolating paths (green), thus leading to metallic transport. d) In a simplified model, having few SWCNTs connected in series, the total resistance of a network can be calculated as a sum over the contact resistances $R_{c,j}$ and internal bundle resistances $R_{i,j}$. In realistic SWCNT-TCFs there are multiple parallel metallic paths, and they must be taken into account by solving the full equivalent resistor system.

Typically, the conductive elements are a mixture of individual tubes and bundles, which consist of several parallel SWCNTs. The structure of the conductive elements has a major effect on the electrical performance of SWCNT networks. The resistance is expected to be dominated by the inter-bundle contacts, rather than resistance along the length of bundles. Therefore, the bundle geometry, together with its electrical properties and network morphology determine the resistance in a specific network [36], [37], [38]. Despite the major role of network morphology and bundle properties for the electrical performance of SWCNT networks, there has been only limited attempts to study the link between these properties. The studies rely on indirect geometrical scaling arguments or fitting of percolation models, which are ill-suited as the typical TCF networks are significantly over the percolation limit [39]. Coleman's group adopted a C-AFM approach in order to directly probe the contact resistance between bundles, although the surfactant based sample fabrication increases the risk of residual surfactants at the contacts, which can lead to significant overestimation of the contact resistances [40]. It has been suggested that the contact geometry has a significant effect on the electrical behaviour of the contacts [35].

2.6 Carbon Coating of SWCNT Networks

Diamond-like carbon (DLC) coatings have been used to improve the wear resistance of bulk materials [41], [42]. DLC is a form of amorphous carbon containing a significant fraction of sp_3 bonds. These coatings could provide a way in which to covalently bond together SWCNTs in the networks forming a hybrid nanomaterial, thus improving mechanical performance while

preserving their native electrical conductivity. DLC-coatings can be fabricated by ion beam deposition, sputtering, plasma deposition, vacuum arc and pulsed laser deposition. The DLC-coatings exhibit dielectric behaviour and could therefore serve as insulating layers in all carbon electronics.

Hydrogen-containing DLC-films were grown on top of dense aligned MWCNT forests and on spin-coated CNT dispersions by means of plasma chemical vapour deposition (PCVD) [43], [44]. The mechanical strength and hydrophobic properties of the MWCNT forests were found to be enhanced. Schittenhelm et.al. used a pulsed laser deposition (PLD) carbon coating process with ion energies of around 100 eV on SWCNT bundles, and were able to maintain metallic conduction while increasing the scratch resistance of the films [45]. However, the detailed characterisation of the formation mechanism, bonding configuration and the optoelectrical and mechanical response of such hybrid nanomaterials has not been carried out.

3 Transparent Conductive Films

3.1 Industry Standard - Indium Tin Oxide

Materials which combine electrical conductivity and optical transparency are essential for thin displays, touch sensors, photovoltaic cells and OLED-devices. Indeed, transparent metal oxides, primarily indium tin oxide (ITO, 90% In / 10% Sn), currently have the industry standard role. ITO has low resistivity when thermally annealed, good transmittance at the visible part of the spectrum, high IR-reflectivity, decent environmental stability and good etchability, which is important for lithographic patterning [46], [47].

However, ITO also has several drawbacks. First, it is fragile and its sheet resistance increases rapidly under repeated mechanical deformation leading in to fracture formation [6]. This limits the applicability of ITO for flexible electronics and prohibits the use of high throughput roll-to-roll manufacturing techniques. Second, ITO has a high refractive index (~ 2) and therefore additional and costly index matching layers are often needed to minimise the Fresnell-reflections [48]. Post-deposition heat treatments are required to increase the size of the crystalline areas for high conductivity ITO-TCFs. Flexible polymer substrates do not withstand the heating and TCF performance on the flexible substrates is from one to two orders of magnitude worse compared to the annealed films [5].

Indium is considered as a critical metal due to its importance in several applications [49]. China, the leading producer of indium, controls over 50% of the annual production, while Japan, Republic of Korea and Brazil produce approximately 10% each. Belgium produces approximately 5% in the EU-region. Total annual production of indium is ~ 640 tons of new resources and ~ 1800 tons including secondary manufacturing from recycled sources [49]. Japan is a major user of indium with approximately 60% of annual consumption. The indium prices have been volatile, increasing from 94 USD/kg in 2002 to approximately 900 USD/kg in 2011. These price fluctuations are explained by the increasing global demand and the supply disruptions stemming from changes in

Chinese strategic metal export quotas [50]. Finding ITO alternatives which are capable of reducing dependence on indium would have a major economic impact both on the LCD-industry with annual revenues of ~ 100 billion USD [51] and on the touch sensor industry with annual revenues of ~ 8 billion USD [5]. A wide range of alternative metal oxide TCFs, such as zinc and tin oxides with different ternary metal dopants like aluminium or gallium, have been studied as ITO alternatives and their performance has improved during recent years. However, the ITO still has a performance advantage, whilst the lack of reliable large area deposition methods for the multicomponent transparent conductive oxides limits their industrial applicability [100].

3.2 Alternative TCF Materials

Carbon nanotubes are a promising alternative TCF material. Various types of CNTs have been used as TCFs, with different pre- and post-deposition treatments and different deposition techniques ranging from direct deposition to contact printing. Wu et al. used vacuum filtration of surfactant-stabilised solution of SWCNTs followed by membrane filter dissolving [1]. The performance of SWCNT films was improved as a result of post-deposition treatment by nitric acid and performance of 30 Ω/sq. at 70% transparency was reported. Other groups have used the surfactant assisted filtration with spray coating reaching 1 kΩ/sq. at 90%, while being limited to 1 cm^2 sample sizes with limited uniformity [24] and with vacuum filtration combined with PDMS contact stamping with arc-tubes, reaching performance of 300 Ω/sq. at 90%, despite rather harsh pre-deposition ultrasound treatment to promote SWCNT-dispersion [52]. Chemical treatments with reagents, such as HNO_3 and $SOCl_2$ have been demonstrated to improve the performance to 500 Ω/sq. at 85% and 300 Ω/sq. at 80% [52],[53].

Diameter and chirality enrichment of specific CNT species has been studied as a potential approach for CNT-TCF performance improvement. The metallic SWCNT enrichment has been demonstrated to improve the TCF performance when compared to mixed networks. However, the short length of the tubes, due to heavy sonication combined with re-bundling during surfactant removal leads to relatively low overall performance with > 1 kΩ/sq. at 90% [54]. Hersham's group demonstrated utilisation of the ultracentrifugation technique for fabrication of DWCNT enriched TCFs. Interestingly, the mechanism explaining the improved optoelectrical performance seems to be the increased length of conductive elements, when DWCNT networks are compared to SWCNT networks fabricated with the same processing techniques. This leads to performances of 146 Ω/sq. and 350 Ω/sq. at 75%, respectively [55]. Whilst Coleman's group studied the effect of different surfactants, SDS and SBS, for arc-synthesised SWCNT networks, the difference was found to be negligible and the TCFs exhibited 110 Ω/sq. at 80% [56]. Other SWCNT deposition techniques such as Meyer's rod coating have also been demonstrated, and while the film performance can be relatively good when strong HNO_3 treatment is used, the complex ink formulation and optimisation processes increase the fabrication costs [57]. The sheet resistance and transmittance values are listed in Figure 3.1 for comparison.

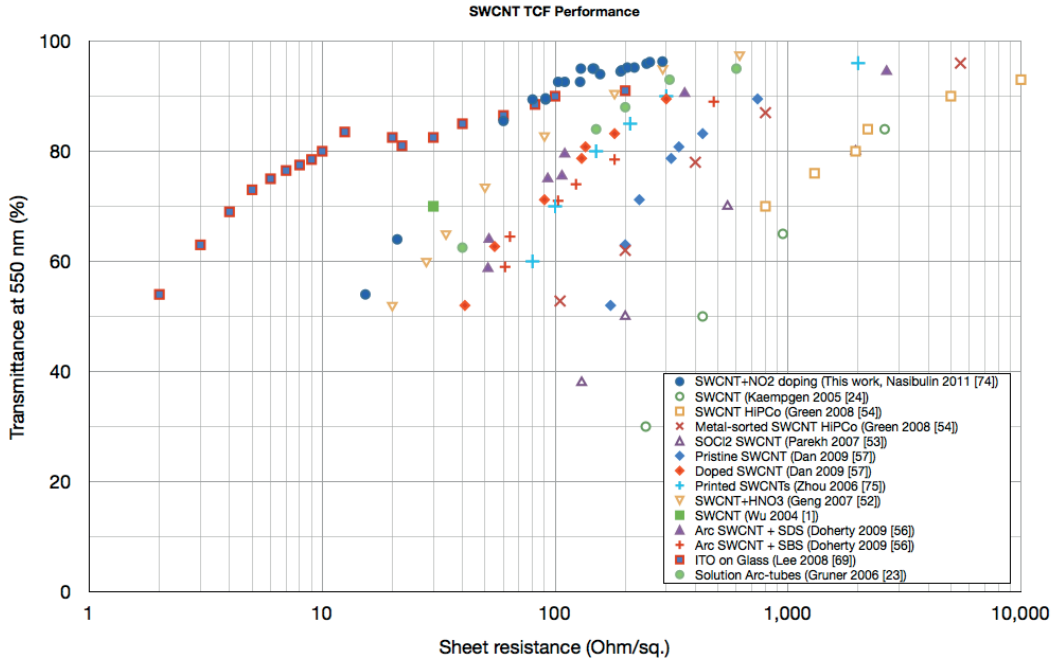

Figure 3.1. The optoelectrical performance of various SWCNT TCF-materials.

Graphene has been also proposed as an alternative TCF material [58], [59]. Theoretically it has a great potential, but in reality crystallographic defects, wrinkles and folds significantly reduce the electrical performance. Different approaches to graphene fabrication are used, including CVD-growth on catalyst surfaces, graphite intercalation, reduction of graphene oxide and graphene flake deposition [60], [61], [62]. The highest performance was reached by CVD-synthesised graphene over planar Cu-catalyst. Large, high performance graphene on Cu-catalyst up to 30 inches in diagonal have been demonstrated, whilst a contact transfer method can be used to transfer the material to flexible polymer substrates. Graphene TCFs can be chemically treated with HNO_3, thus reaching an optoelectrical performance of 30 Ω/sq. at 90% [63]. This optoelectrical performance level is remarkably high and has proven to be difficult to reproduce whilst values around 300 Ω/sq. at 85% are more typically reported [64]. Solution processing of reduced graphene oxide flakes has been recently demonstrated to reach sheet resistances of 800 Ω/sq. at 82% [65]. High performance graphene TCFs requires annealed large area Cu-catalyst. Annealing and growth processes last hours and requires vacuum processing [63]. In addition, the high performance graphene is transferred to the substrate material by etching the catalyst layer, thus increasing the material consumption and processing costs when compared to simple, ambient pressure and low temperature preparation of SWCNT TCFs.

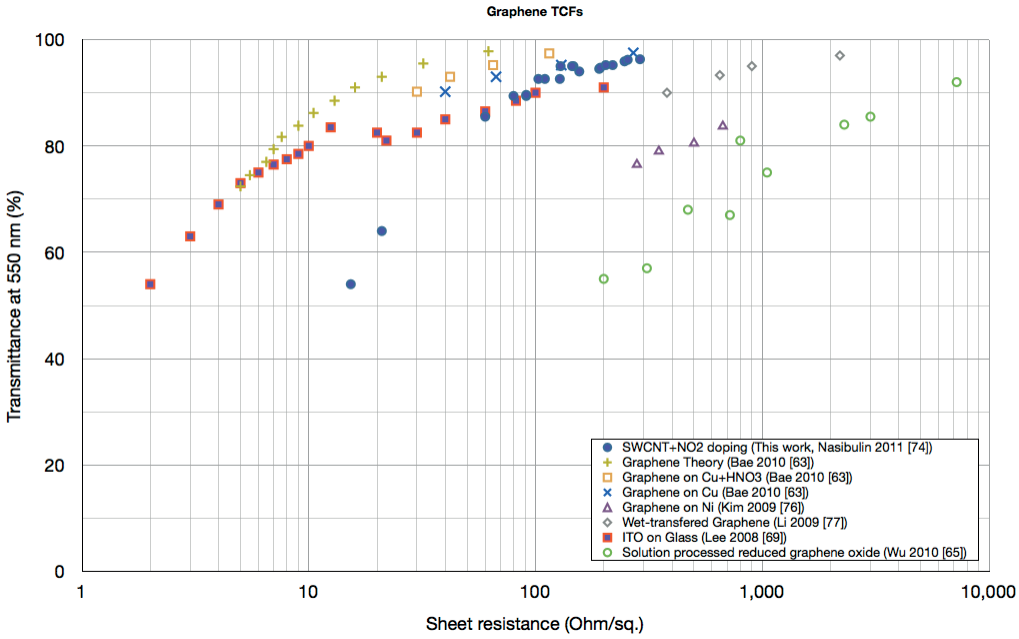

Figure 3.2. The optoelectrical performance of various graphene based TCFs.

Metal nanowires and metal gratings provide a good electrical performance for the current-driven devices, while the maximum transparency is limited. Whilst both silver and copper nanowire TCFs have been demonstrated, the Cu-nanowire networks suffer from severe oxidation in ambient conditions [66], [67]. Ag-nanowires are also prone to oxidation, although the problem is less severe and can, to some extent, be reduced by protective coatings [68]. Lee et.al. have demonstrated Ag-nanowire networks with sheet resistance of 16 Ω/sq. at 86% transmittance [69]. Careful removal of the surfactant is required to reach the reported performance. Macroscopic silver films have also been reported but they have a very limited maximum transmittance [69]. Patterned Ag-gratings can be fabricated by, for example, nano-imprinting lithography. Depending on the dimensions of grid and metal trances the optical transparency and electrical conductivity of the TCF can be varied. Zou et al. demonstrated gratings with a sheet resistance of 9.1 Ω/sq. at 78% transmittance [70]. It is worth noting that the nano-structured metal TCF exhibit relatively high surface roughness when compared to ITO and nanocarbon TCFs, which can be detrimental to applications such as organic solar cells, where increased roughness can lead to shunting through the active layers [71]. In addition, various conductive polymers have been studied as alternative TCF materials. The highest performance has been achieved with PEDOT:PSS, which requires chemical doping and post-deposition treatments to improve the conductivity to an acceptable level and are prone to environmental degradation [72], [73]. The performance of these other alternative TCF materials is summarised in Figure 3.3.

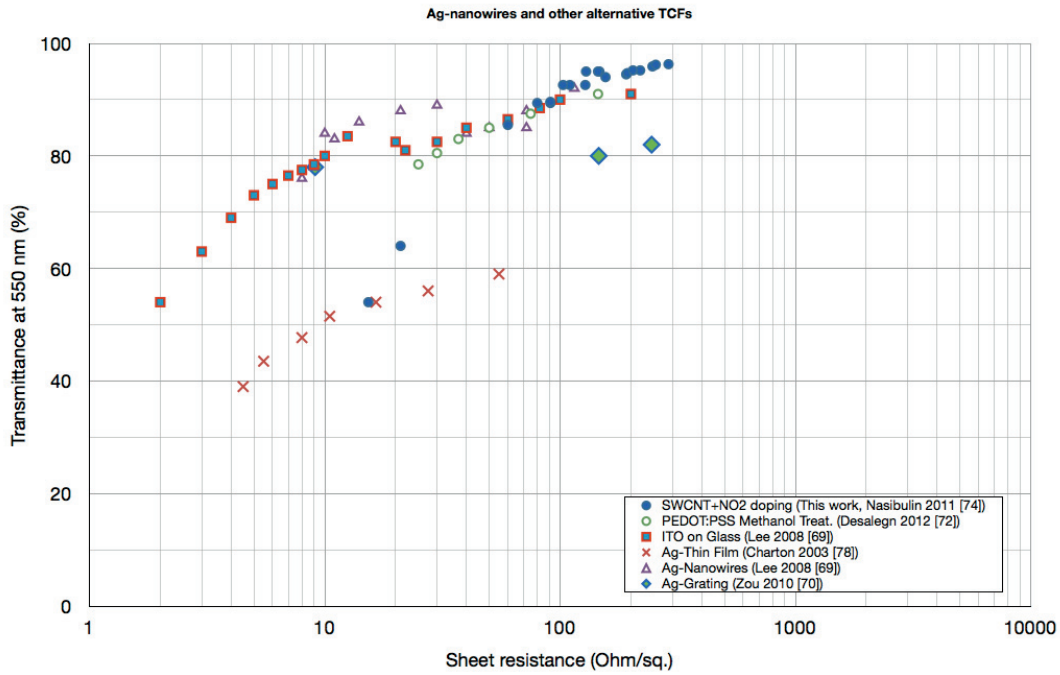

Figure 3.3. The optoelectrical performance of silver nano-wires and conductive polymers might provide feasible alternatives for ITO and carbon nanomaterials based solutions for current-driven devices, given that the environmental stability of these novel solutions is to be improved.

4 Methods

4.1 Aerosol-CVD Synthesis

In this thesis an aerosol-CVD technique was used for the synthesis of SWCNTs [20]. The process is based on thermal decomposition of ferrocene and subsequent formation of iron nanoparticles. This is followed by disproportionation of the carrier gas and carbon source, carbon monoxide (CO), on the surface of the catalyst, leading to SWCNT growth. The experiments were carried out in two different reactors, the first being a lab-scale development reactor and the other a pilot-scale reactor, which provided significantly larger growth volume leading to longer SWCNTs and bundles (Publication 1).

The lab scale reactor was used for the initial optimisation of the synthesis conditions before the transition to pilot-scale reactor. The reactor consists of a ferrocene saturator, a water-cooled gas injector probe, and a heated tube furnace with variable maximum temperature ranging from 800 to 1200 °C. A main flow of CO (300 cm^3/min, Chemical Carbon Monoxide, 99 vol-%, AGA) is controlled by a metering valve and a critical orifice calibrated against a bubble flow cell (Gillian Gilibrator). The main flow is passed through the ferrocene cartridge, which is filled with ferrocene powder mixed with silicon dioxide granules (99%, Strem Chemicals and 99.9%, Balzers Materials, weight ratio ferrocene:silicon dioxide = 1:4) to provide the conditions for ferrocene vapour

saturation (partial pressure 0.8 Pa at room temperature). The growth chamber consisted of an alumina tube with an internal diameter of 22 mm and a length of 550 mm and was placed inside the tube furnace (Entech, Sweden). The flow containing ferrocene vapour was introduced directly into the high-temperature zone of the reactor through the water-cooled probe (water temperature of 24 °C) inserted 6.5 cm deep into the reactor.

An additional CO flow of 100 cm^3/min was introduced into the reactor between the water-cooled probe and the reactor tube in order to reduce recirculation near the cooled injector tip [20]. The reactor temperature profiles were separately characterised by thermocouple measurements. In addition, a small flow of carbon dioxide (up to 10 cm^3/min) was introduced to the reactor when operated in the lower end of the temperature range to promote SWCNT formation [79]. The additional CO_2 flow was controlled by mass flow controllers (Aalborg Systems, USA) and was mixed with the main flow after the ferrocene cartridge. The lab scale reactor is schematically depicted in Figure 4.1. Ferrocene is thermally decomposed in the temperature gradient formed in between the cooled injector probe and the heated reactor walls. The decomposition leads to supersaturated conditions which result in iron nanoparticle formation. Carbon monoxide gas is decomposed on the formed iron catalyst particles, leading to SWCNT growth [20]. The SWCNTs are collected downstream from the reactor by membrane filtration [80].

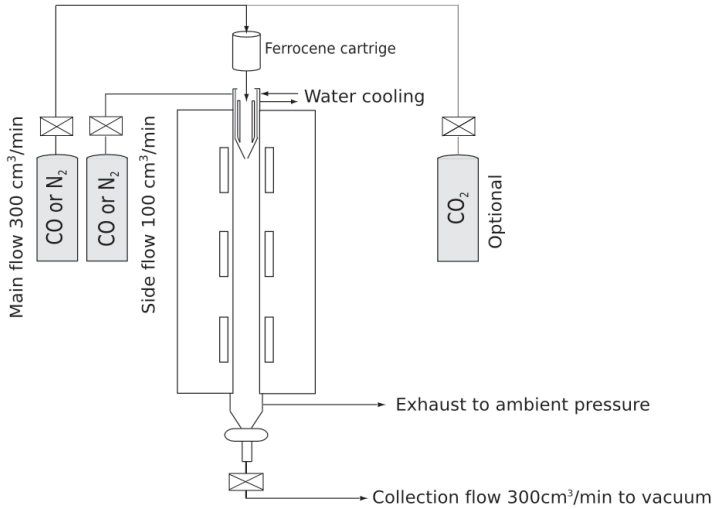

Figure 4.1. The flow schematics of the lab scale ferrocene reactor. The main CO flow is passed through the ferrocene cartridge and mixed with optional CO_2 flow. This flow is injected into the heated (880 °C - 1050 °C) tube furnace. Additional side flow of CO is injected between the reactor tube and water-cooled injector to prevent recirculation. The reactor exhaust is open to ambient whilst the sampling is carried out using flow rate controlled vacuum filtration.

The pilot-scale reactor was based on the same operating principle while the physical dimensions and the production capacity is larger. The reaction chamber was 150 mm in diameter and 1.5 m in length. The reactor was operated at a total CO flow rate of 4 l/min and at a temperature of 880 °C. The SWCNT growth took place inside the heated reaction chamber which was maintained at maximum temperature of 880 °C, based on the optimisation carried out in the lab-scale reactor.

The synthesised SWCNTs were collected downstream of the reactor by filtering the aerosol through a nitrocellulose membrane filter to form a SWCNT network (Millipore, HAWP, 0.45 μm or 1.2 μm pore diameter). The networks were transferred from low adhesion filters to various substrates by the developed room-temperature press transfer process, which is described later in thorough detail. The press transfer method is compatible with roll-to-roll fabrication, thus opening up further scaling potential in industrialised production.

4.2 Materials Characterisation

Sheet resistance is an important parameter of thin conductive films (TCFs). It can be evaluated for uniform TCFs directly with a four point probe, without thickness measurement. To link the sheet resistance, resistivity and dimensions of the sample, a simple rectangular system with resistivity ρ, thickness t, length L and width W was considered. The resistance of the system, R, is expressed by using the classic definition of resistivity:

$$R = \frac{\rho L}{A} = \frac{\rho L}{Wt} = (\rho / t)(L / W) = R_s(L / W) \ , \qquad (4.1)$$

where R_s is the sheet resistance of the system. While the sheet resistance has the same units as resistance (Ω), Ohm per square (Ω/sq.) is used to highlight the interpretation of sheet resistance as resistance over a fixed aspect ratio sample area. The random orientation of SWCNTs in the typical networks justifies the use of the isotropic conduction model. In case of partially aligned SWCNT networks the resistance will be lower in the direction parallel with the alignment direction due to the smaller number of resistive inter-bundle contacts per unit length.

For low resistance samples the four point measurement had to be used to eliminate contributions of the probe-sample contact resistances [81]. The idea was to separate the current carrying (low impedance) circuit and the voltage sensing (high impedance) circuits, as depicted in Figure 4.2. Current flowing in the high impedance circuit is negligible and thus the voltage drop takes place in the resistance being measured. The contact resistances in the high impedance circuit do not contribute to the measured resistance, which is calculated by using Ohm's law V = R*I.

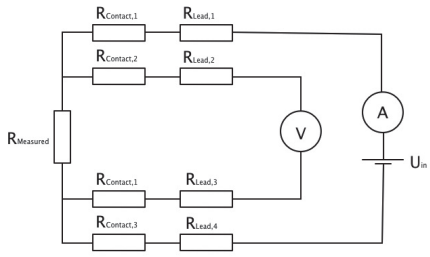

Figure 4.2. The basic principle of the four point measurement. The current is supplied by a separate circuit (outer leads #1 & #4) to resistor to be measured, while the voltage drop over the resistor is measured by another electrical circuit (leads #2 & #3), where the high input impedance limits the current to a negligible level and thus largely eliminates the effect of the unknown contact resistances. Here $R_{measured}$ is the resistor under measurement and $R_{Lead,i}$ are the resistances of the measurement leads. $R_{Contact,i}$ are the unknown contact resistances between the probe and the sample.

In this work the sheet resistances were characterised using a linear four point probe (Jandel, Jandel-Engineering Ltd., England) combined with a four terminal multimeter (Agilent 34411, Agilent, USA). In the linear four point probe the sharp spring loaded (radius of curvature 100 μm, load 60 g) tungsten tips were arranged in a row at 1.0 mm distances. The measurement current was applied to the outer probes and the voltage drop was measured in between the inner pair of probes. For a linear probe the sheet resistance can be evaluated from relation:

$$R_s = (\rho / t) = \frac{\pi}{\ln(2)} \frac{V}{I} \approx 4.532 \frac{V}{I}, \qquad (4.2)$$

where V is the measured voltage between the centre probes and I is the current through the sample [81]. The expression is valid when the sample dimensions are much larger than probe separation. For SWCNT characterisation the samples were press-transferred to a substrate, which supported the TCF during the measurement whilst the probe-needle unit was pressed to the substrate through the use of a vertical translation stage.

Optical absorption spectroscopy was also used for the SWCNT TCF characterisation. For full wavelength absorption, spectroscopy samples were transferred to optically transparent quartz substrates (1 mm HQS300 Heraeus), and a clean substrate was placed on the reference beam for the purpose of substrate contribution elimination. Measurements for freestanding SWCNT films were performed with an empty reference beam. A Perkin-Elmers Lambda 950 UV-Vis-NIR spectrometer was used to measure the absorption spectra. The instrument allows for sample characterisation in between 175 nm and 3300 nm wavelengths by using two excitation sources (deuterium and halogen lamps). Raman spectroscopy was carried out with a Wintech Alpha 300 Raman spectrometer equipped with Nd:YAG laser operating at 523 nm or with Horiba Jobin Yvon LabRam spectrometer using a 633 nm excitation laser.

Scanning electron microscopy (SEM) was used for the characterisation of the network morphology and bundle lengths of SWCNT samples. The SEM characterisation in this work was carried out with JEOL JSM-7500F and Zeiss Sigma VP microscopes. Transmission electron microscopy (TEM) provides greater resolving power than SEM and can be used for the characterisation of individual SWCNT characteristics, such as tube diameter and chirality down to atomistic resolution [82]. The TEM measurements in this work were carried out with a JEOL-2200FS double aberration-corrected microscope, operated mainly at 80 kV. TEM samples were deposited on TEM grids (Holey Carbon Film 400 Mesh CU, Agar Scientific, UK) by placing the TEM grids on a nitrocellulose filter typically for a 15 s deposition.

4.3 Conductive Atomic Force Microscopy

Atomic force microscopy (AFM) is based on the utilisation of a very sharp tip with a radius of curvature in the order of 10 nm on a flexible cantilever for nanoscale imaging or manipulation. The tip is scanned over the surface by moving the sample with a piezoelectric stage. The cantilever flexes when interacting with the sample surface according to Hooke's law. The tip deflection is

detected by a position sensitive photodiode-array, which measures movement of a laser beam reflected from the cantilever. The tip can be scanned in contact mode touching the sample surface. Alternatively the scanning can take place in non-contact mode, when the tip is vibrated slightly over the resonant frequency at a few nanometers above the surface whilst van der Waals forces between the surface and tip reduce the resonant frequency. Scanning can also be performed in tapping mode, when the tip is vibrated closer to the sample surface and touches the surface briefly during each cycle.

In this work an atomic force microscope was used to study the electrical characteristics of inter-tube and inter-bundle contacts. By using a conductive tip and cantilever, the system allowed for the spatially resolved biasing of SWCNTs, identification of contact location, morphology and contacting tube or bundle diameters. The conductive tip durability is essential for experiments which require extensive imaging at high resolution and a reliable electrical contact for IV-curve measurements. Metal coated tips were used, although the coating is prone to damage, which is detrimental for both the imaging resolution and the reliable contacting for electrical characterisation. Highly doped diamond tips were used to overcome these problems. They combine high hardness, conductivity and durability, thus reducing the likelihood of tip damage (Nanosensors DT-NCHR, Nanoworld AG, Switzerland). The schematic of the measurement setup is shown in Figure 4.3.

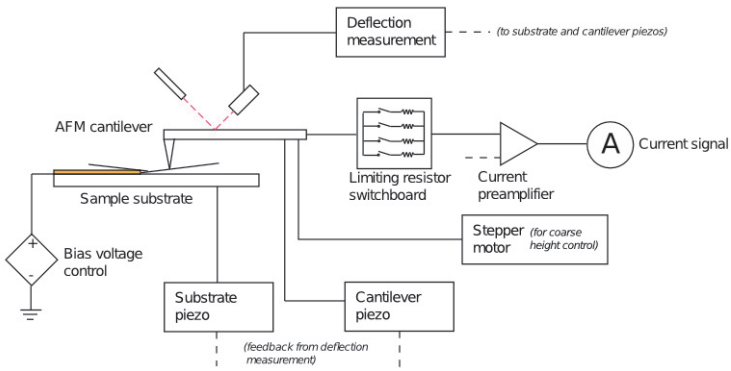

Figure 4.3. A schematic view of a C-AFM measurement system. Conductive tip and bias source and sensing electronics are installed to a standard AFM-setup. In this case both imaging and electrical measurement control functions are integrated with a Labview-based measurement software.

The samples were fabricated on highly p-doped Si:SiO_2 substrates with a 250 nm thick oxide. For SWCNT network biasing an Au-electrode was fabricated on the chip (chip 10 mm * 10 mm, electrode approximately 3 mm * 3 mm). The chip area outside the electrode was masked and 40 nm of Au was evaporated on a 5 nm thick Ti layer by using an electron beam evaporator (Custom made Instrument, Model IM9912 Micronova Cleanroom, Aalto University). C-AFM measurements require high sample cleanliness to maintain both the imaging resolution and to minimise tip-sample contact resistance. After the electrode deposition the mask was removed and the samples were cleaned with sonication in acetone, followed by an isopropyl alcohol rinse and oxygen plasma cleaning. The chips were then placed on a 47 mm nitrocellulose filter, which was connected to the

pilot reactor whilst a sub-percolating SWCNT network was deposited on the chip surface by diffusion. The network morphology and contact density was evaluated with SEM-imaging prior to C-AFM characterisation.

For the contact resistance measurements, the Au-electrode was wire bonded to a chip carrier to allow for biasing with the C-AFM system (Veeco Dimension 500 AFM). An area near the Au-electrode edge was initially imaged in non-contact mode to locate suitable, isolated SWCNT contacts. If one of the contacting branches was connected to the electrode via several paths, the contact was isolated by approaching the surface while applying a high bias. This procedure destroyed the tube near the approached point, as verified by imaging and electrical measurements. When the suitable contact was accessible, the tip was brought in to contact with the secondary branch further away from the electrode and IV-curves were recorded. The primary branch was contacted after performing a second imaging scan and the resistance was evaluated in a similar way to that of the secondary branch. The contact resistance was calculated from the difference between the secondary and primary branches, as indicated in Figure 4.4. b). Measurements were performed approximately 0.5 µm away from the contact so as to prevent contact modulation by the approaching tip. Each of the branches can either be an SWCNT (diameter < 2.4 nm) or a small bundle of SWCNTs (diameter > 2.4 nm) [30], both referred to as SWCNTs. Measurements were also performed to estimate the resistance along bundles, by recording the IV-curves in locations at 1 µm increments as shown in Figure 4.4. c). The two main morphologies of SWCNT contacts, "X-type" and "Y-type", are shown in Figures 4.4. d) & e).

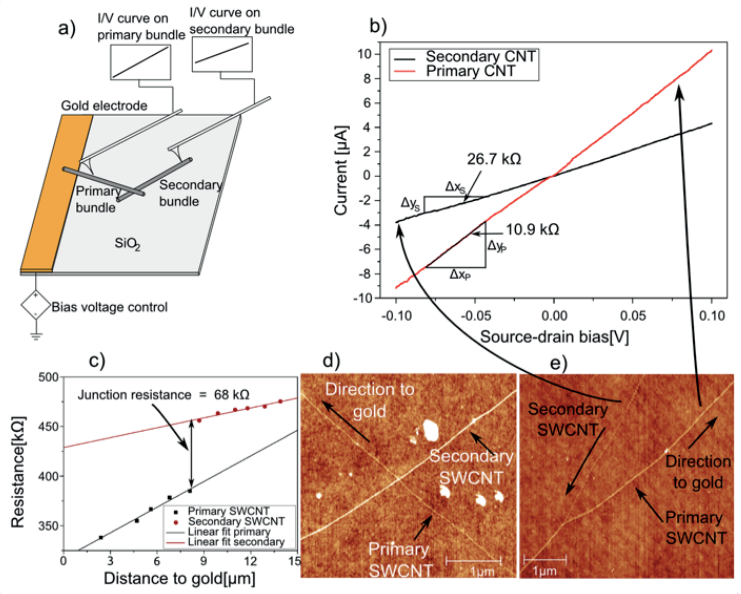

Figure 4.4. The measurement configuration for bundle-bundle contact resistance estimation. a) Measurement layout: A combination between tapping and contact mode is used to image and probe the local electrical properties of isolated SWCNT junctions near the Au contacts. b) Contact resistance is estimated based on the difference between IV-curve slopes on secondary and primary tubes c) length resistance along tube is estimated by measuring multiple IV-curves on different locations along the tube, typically with 1 µm increments. Tapping mode images of d) X- and e) Y-junctions (Publication 3).

4.4 Dye-sensitised Solar Cells

Dye-sensitised solar cells (DSC) were studied as a potential application for SWCNT-networks. A DSC consists of three main components: photo-electrode, counter-electrode and electrolyte. The photo-electrode is a layer of TiO_2 nanoparticles, covered by a ruthenium polypyridine dye on a conductive surface, such as fluorine doped ITO (FTO). The counter-electrode is a conductive surface with catalyst material like platinum. An iodine/tri-iodine redox complex inorganic solvent is typically used as an electrolyte. Light is passed to the dye material, where the photons excite the electrons which flow to TiO_2. The electrons diffuse through the electrolyte to the electrode, then to the external electric load in the circuit and back to the DSC counter electrode. The oxidised dye-molecule is regenerated by the iodine ions in the electrolyte, oxidising those into tri-iodine, which diffuse to the counter electrode where they are reduced to iodide, as shown in Figure 4.5.

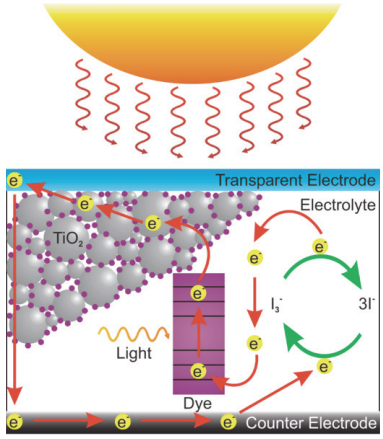

Figure 4.5. The basic operation of a dye-sensitised solar cell (adapted from Wikimedia Commons as public domain [83]).

SWCNT films can be used as a catalytically active, conductive and flexible counter-electrode material to replace the platinum catalyst on FTO-glass. The SWCNT network can be coated by other materials such as PEDOT, so as to further enhance the catalytic activity towards the tri-iodine reduction reaction. Carbon nanotubes have, thus far, received only limited attention due to the low observed catalytic activity [84]. The SWCNT films used here were synthesised by using the pilot-scale reactor, following which they were transferred to PET substrates before being subjected to ethanol densification. The films were characterised prior to the cell assembly by absorption spectroscopy, sheet resistance and SEM measurements. The iron catalyst particles, which are detrimental for DSC stability, were removed electrochemically by anodic stripping in 1 M HNO_3 [85]. For PEDOT deposition, an aqueous solution of EDOT, was electropolymerised to the surface. The overall solar cell assembly process followed the standard procedure described in detail in the previous articles [86], [87].

For determination of the energy conversion efficiency, IV-measurements were performed in a solar simulator. The light intensity used was 1000 W/m^2, AM1.5G i.e. equivalent to the sun spectrum through an air layer with 1.5 times the thickness of Earth's atmosphere when the Sun is in zenith.

The solar cell efficiency, η, is calculated by dividing the maximum power point by the incident light power,

$$\eta = \frac{P_{MAX}}{P_{IN}} = \frac{I_{MPP} V_{MPP}}{P_{IN}}, \tag{4.3}$$

where P_{MAX} is the maximum power from the cell, and I_{MPP} and V_{MPP} are the current and voltage in the maximum power point and P_{IN} is the input light power. Short circuit current, I_{SC}, open circuit voltage, $V_{OC,}$ and fill factor, *FF*, are other important performance parameters for a solar cell. The fill factor represents the fraction of converted power compared to an optimal cell with square IV-curve. The fill factor is defined as:

$$F.F. = \frac{I_{MPP} V_{MPP}}{I_{SC} V_{OC}}. \tag{4.4}$$

4.5 Carbon Coating of SWCNT Networks

PVD-formed carbon coatings were studied as a way to improve the mechanical properties of SWCNT-Ns. The carbon coatings were deposited using a pulsed vacuum arc without energy filtering. A 2.6 mF capacitor bank was charged to 200 V and the arc was triggered with ignition electrodes. The maximum pulse current was 3 kA and the pulse half width was approximately 150 μs. Each pulse was triggered separately at 1 Hz frequency. The deposition rate during the pulse was around $1.4*10^{15}$ ions/cm^2, as measured from the growth rate of a carbon layer on a flat silicon substrate. The distance from the cathode was approximately 300 mm. The average carbon ion energy was measured as 40–50 eV using an electrostatic probe [88].

For in situ electrical resistance characterisation, a rectangular SWCNT sample was prepared on a PET-substrate. Copper conductors were attached to both ends of the sample area using commercially available silver paint, and connected to an external multimeter (Fluke 88). The sample was measured after the coating process to study the impact of ambient adsorbates and the subsequent recovery of sheet resistance. To extract electrical characteristics of pristine and carbon coated SWCNT samples on PET and Si substrates, a four point probe and a digital multimeter were used for the sheet resistance measurements.

An approximately 20 nm thick carbon coating was then deposited on to a segment of the network. Indentation was carried out with a nano-mechanical testing system (TriboIndenter TI-900, Hysitron, Inc.). Arrays of indents with varying maximum loads were performed on both the coated and the uncoated SWCNT-Ns with the peak-load range varying from 20 to 200 μN. The indenter was a Berkovich-type with a nominal tip radius of 130 nm. The tip scanned a selected area on the sample surface for nanowear experiments. The worn surface on the coated and non-coated network was examined by studying the scanning probe microscopy (SPM) images in assistance with SEM observation. The amount of wear and material deformation and displacement were estimated by comparing the 3D-reconstructions of surface profiles before and after nanowear experiments.

5 Results and Discussion

5.1 Optoelectrical Performance of SWCNT Networks

First, to improve the optoelectrical performance of SWCNT networks, the synthesis reactor conditions were optimised. The optimisation was based on previous studies which suggested that the electrical performance of a SWCNT network is controlled by the highly resistive inter-tube and inter-bundle contacts [89], [40]. Therefore, if the bundle length could be increased, it should reduce the number of resistive contacts and thus reduce the overall electrical resistance of a SWCNT network. To study the relation between the network morphology and the electrical performance of SWCNT, TCFs were fabricated with different reactor conditions, thus leading to mean bundle lengths of 1.3 ± 0.8, 3.3 ± 1.4 and 9.4 ± 1.4 μm, as shown in Figure 5.1. The bundle lengths were estimated based on statistical analysis of SEM-micrographs of low density networks (Publication 1). The shortest tubes were synthesised with maximum reactor temperature of 1050 °C and based on previous in-situ sampling studies in the same lab-scale reactor, the catalytic CO-decomposition reaction was thermodynamically inhibited in temperatures above 945 °C [90]. When the reactor maximum temperature was increased above this temperature, the active growth zone was limited to the area just bellow the gas injector, where the temperature is reduced and thus the bundles are the shortest. The medium length bundles (3.3 μm) were synthesised in the same lab-scale furnace at a lower temperature of 880 °C to avoid inhibition of the CO-disproportionation reaction and SWCNT growth termination. The longest bundles were synthesised in a pilot-scale reactor maintained at 880 °C, which offered a significantly longer growth zone when compared to the lab scale reactor. A 1 % volumetric fraction of CO_2 was added to the CO-flow at the inlet of the reactor to enhance the catalyst particle activity [79], for both reactors when run at 880 °C. The diameter distributions of the SWCNT-Ns were analysed with optical absorption spectroscopy whilst the mean SWCNT diameters ranged from 1.4 to 1.7 nm [91], [92]. The SWCNT had dominantly high chiral angles, near the armchair edge [93]. For the morphology estimation the bundle diameters were estimated based on statistical analysis of TEM images (Philips CM200 FEG) whilst the bundle length was estimated by SEM imaging of very sparse networks, where the individual bundles were well separated, thus allowing length estimation.

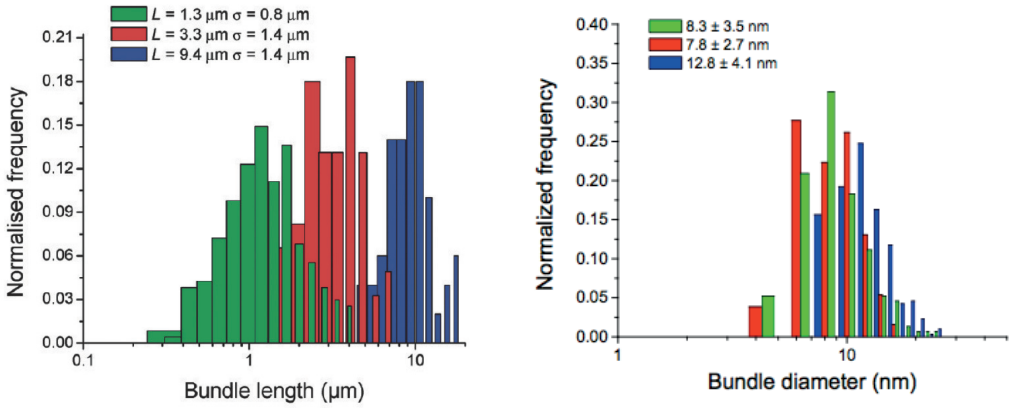

Figure 5.1. The bundle length, as estimated from the low density samples, can be modified by over large range by changing the synthesis reactor conditions (Publication 1).

The optoelectrical performance characterisation was carried out by varying the SWCNT network collection times, thus leading to different network density, sheet resistance and transmittance. The results are shown in Figure 5.2. The strongly overlapping bundle diameter distributions suggest that the bundle diameter changes cannot explain the performance differences. However, the sheet resistance was found to be strongly dependent on the average bundle length in the respective reactor condition. The sheet resistance of the sample containing the shortest bundles (1.3 µm) was 22 kΩ/sq. at 90% transmittance. The samples with longer bundles (3.3 and 9.4 µm) yielded SWCNT networks with 2700 and 820 Ω/sq. respectively at 90% transmittance. The increase in the bundle length meant a significant increase in the performance of SWCNT TCF, but alone it was not sufficient to make the pristine SWCNT networks competitive with ITO on plastic, which typically exhibits a sheet resistance around 100 Ω/sq. slightly bellow 90% transmittance at 550 nm.

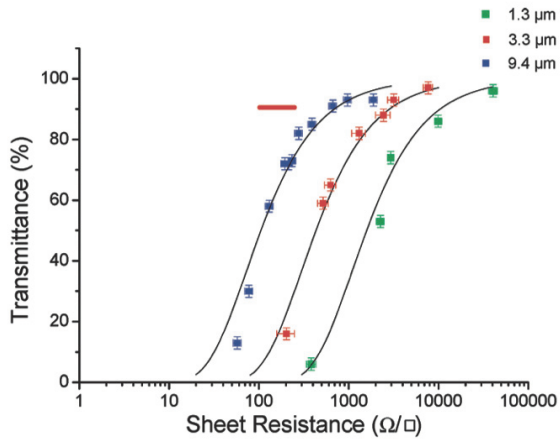

Figure 5.2. Increasing bundle length correlates strongly with improved optoelectrical performance in case of pristine networks. However, this alone is not sufficient to make the films competitive with the ITO-on-plastic (red bar), which typically has sheet resistance of around 100 Ω/sq. at 90% transmittance (Publication 1).

5.2 Chemical Treatment of SWCNT Networks

To further reduce the sheet resistance of the SWCNT networks, a fast liquid-based post-deposition treatment was developed. The SWCNT network was first densified by wetting the film through the drop casting of ethanol, followed by solvent evaporation in an ambient atmosphere. During the evaporation, the SWCNT network is compressed in the out-of-plane direction by the surface tension of the solvent. The densification process modifies the network morphology by increasing the network connectivity and by forming significantly larger bundles as can be seen from the comparative SEM imaging in Figure 5.3. It is worth noting that the post deposition treatment can change the bundle and network morphology, when compared to the pristine, low density SWCNT-Ns used for SEM length analysis.

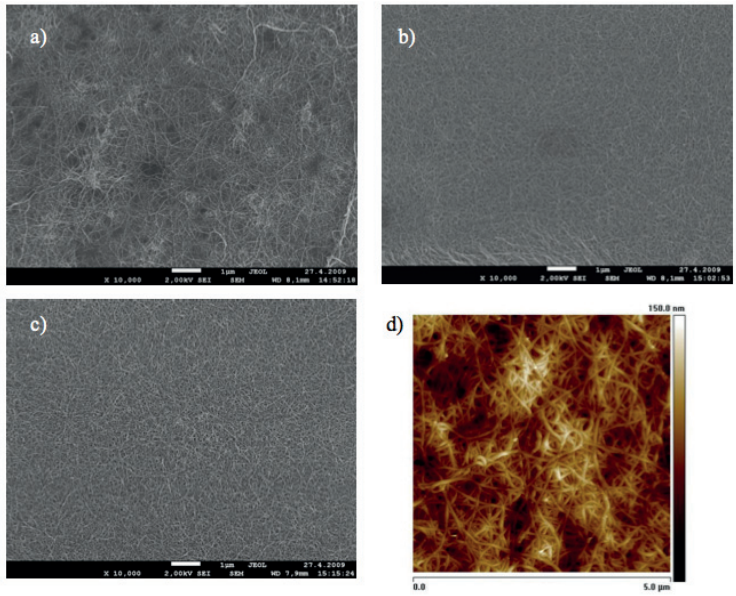

Figure 5.3. The liquid post-deposition treatments have a strong effect on the network morphology of the SWCNT networks, as can be seen from SEM and AFM scans of a) pristine, b) ethanol densified and c&d) densified and HNO3 treated SWCNT networks (Publication 1).

The densification was combined with rapid nitric acid treatment. The SWCNT network was dipped into concentrated HNO_3 for 60 s, followed by de-ionised water rinsing for 15 s to remove the remaining acid. The treatment was performed to chemically dope the semi-conducting SWCNTs and to decrease the inter-bundle junction resistances [40]. The liquid treatment helps to improve the optoelectrical performance of the SWCNT TCF significantly, and the best SWCNT-Ns from the pilot-scale reactor exhibited sheet resistances as low as 110 Ω/sq. at 90% transmittance, making the chemically treated SWCNT TCFs' performance competitive with the commercial ITO on plastic films [94], [95]. When compared to other studies, the HNO_3 treatment used here was significantly faster, with a reaction time of 1 min, when compared with the reaction durations of 15 min, 60 min and 3 h used with previous liquid based purification and densification approaches [96], [52], [53]. These studies suggest that the stability of the nitric acid is limited when exposed to the ambient conditions and that the sheet resistance can increase up to tens of percents during a few weeks of ambient exposure. While the ageing effects were not studied in detail in this thesis, a similar effect

was observed in these samples with around 20% sheet resistance increase during two weeks storage in ambient conditions. However, when used in applications such as touch sensors, the chemically treated SWCNT-TCFs will be laminated with other components of the display stack, which protect the treated SWCNT-Ns and help to stabilise the performance. The effect of the post-deposition treatment was confirmed with UV-vis-spectroscopy as indicated in Figure 5.4 and by Raman-spectroscopy in Figure 5.5.

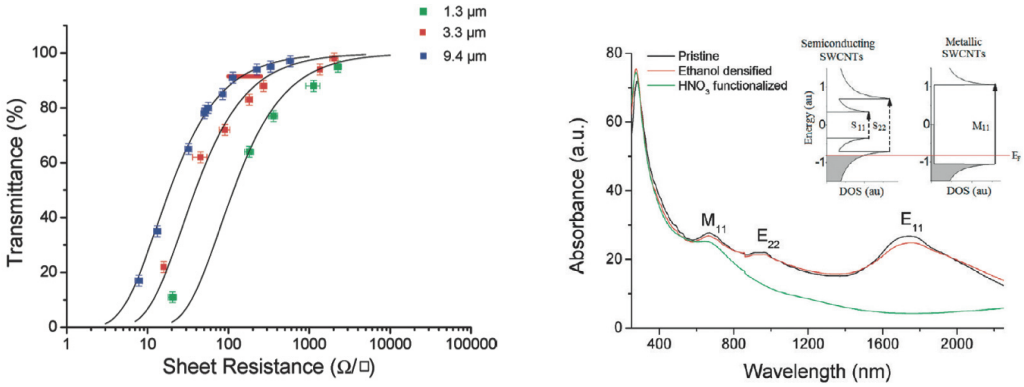

Figure 5.4. The optoelectrical performance of the ethanol densified and HNO_3 treated SWCNT TCF is greatly improved when compared to pristine TCFs, making the materials performance competitive with the ITO-on-plastic. Despite the short HNO_3 treatment time, the treatment effect can be verified by the suppression of E_{22} and E_{11} transitions, and suppression and upshifting of the G-band in the Raman-spectra (Publication 1).

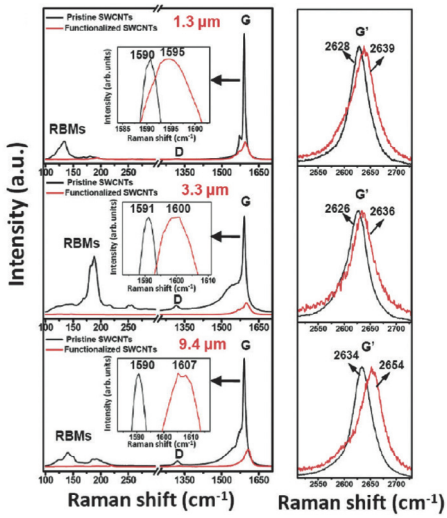

Figure 5.5. The Raman-spectra obtained from pristine, as deposited and from HNO_3-treated SWCNT-Ns, synthesised with different reactor conditions. The acid treatment significantly reduces the Raman-signal intensity and results in upshift of G-band, indicating P-type effect (Publication 1).

One of the main hypotheses of this work was that the resistive contacts between tubes or bundles are dominating the resistance of SWCNT networks, which is supported by the observation of reduced sheet resistance with increasing bundle length. The nitric acid post-deposition treatment

is an effective way in which to further reduce the sheet resistance and the mechanism of the improvement should be analysed. By comparing the relative resistance improvement, which is calculated as average of ratios of pristine and acid treated sheet resistances, it can be seen that the nitric acid treatment has the largest impact on the samples with the shortest mean bundle length. As the bundle length increases, the relative improvement with the post-deposition treatment is reduced, reaching its minimum with the longest bundles as indicated in Table 5.6. This indicates that the acid treatment improves the conductivity by lowering the contact resistances between bundles. If the treatment would modulate the bundles' internal conductivity, the effect should be similar for the samples with different bundle lengths, as the overall length of conductive paths does not change if long bundles are replaced by shortened segments.

Table 5.6. The average improvement by post-deposition treatment decreases with increasing bundle length. This suggests that the post-deposition treatment mainly modulates the bundle-bundle contact resistance as the contribution of possible internal bundle resistance should be independent of the bundle length. The average resistance improvement is calculated as average of ratios of pristine and acid treated sheet resistances at constant transmittance as averaged point-wise comparison.

$\Delta R_S = R_{s,prist}/R_{s,HNO3}$	Bundle Length
13 ± 3	(1.3 ± 0.8) μm
7 ± 2	(3.3 ± 1.4) μm
5 ± 1	(9.4 ± 1.4) μm

During the later stages of the research the pilot-scale reactor was further optimised and an improved chemical treatment method was developed (Publication 2), thus allowing for an additional reduction of the sheet resistance. For the gas based chemical treatment the SWCNT thin films were ethanol densified and treated with gas-phase NO_2 with a performance of 84 Ω/sq. at 90% transmittance achieved, as shown in Figure 5.7. As the chemical groups responsible for the resistance reduction are identical for both the nitric acid and NO_2 gas, the improved performance is likely to be explained by increased bundle length, even though the length distribution was not carefully analysed for this case. Pristine aerosol-synthesised SWCNT networks have a lower sheet resistance than networks fabricated from arc, laser or HIPCO SWCNTs, thus indicating the high intrinsic quality of aerosol-CVD SWCNT networks. Chemically treated SWCNT-Ns have better performance than other reported studies, where chemically modified SWCNT and DWCNT networks have been used. The elimination of harsh cleaning and dispersion steps and surfactants, which are difficult to remove after network formation, combined with rapid acid treatment help to maintain the good intrinsic quality and long bundle length of aerosol-CVD SWCNTs. The optoelectrical performance matches the typical performance of ITO on polymer substrate, and thus makes the SWCNT networks based transparent conductive films competitive with ITO on flexible substrates in terms of optoelectrical performance.

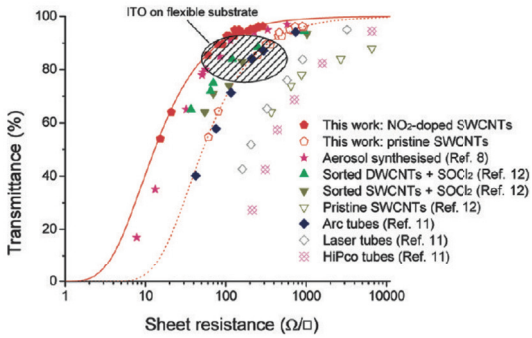

Figure 5.7. Further optimisation of the synthesis reactor chemistry and chemical treatment helped to further improve the optoelectrical performance of SWCNT TCFs in order to yield sheet resistances as low as 84 Ω/sq. at 90% transmittance (Publication 2). The references presented in the image are from the original publication.

5.3 Contact Resistance Estimation with Conductive-AFM

Conductive atomic force microscopy (C-AFM) enabled analysis of the contact morphology and bundle diameters combined with electrical contact resistance estimation. Furthermore, by performing multiple measurements at different locations along a SWCNT bundle, the resistance per unit length was estimated.

Figure 5.8 shows the contact resistances as a function of primary and secondary SWCNT diameters as well as the intersecting angle for a number of X- and Y-contacts. All contact resistances of SWCNTs with diameters from 1 to 10 nm, were found within a range of 29 kΩ to 532 kΩ. Y-type junctions exhibited significantly lower contact resistance than X-type junctions whilst the contact resistance decreased with increasing bundle diameter (Figure 5.8). Figure 5.9 a) shows a histogram of the contact resistance for all X- and all Y-contacts. The behaviour of contact resistance with the diameter of SWCNTs was in contrast with a previous study by Nirmalraj et al., which suggested that SWCNT junction resistance is directly proportional to the diameter of SWCNTs [40]. It is worth noting that they observed mainly large diameter SWCNT bundles, and that the difference between the experiments could be explained by the presence of SDS surfactant or other residual contaminants in their SWCNT samples, whereas this was not the case with the surfactant-free deposition.

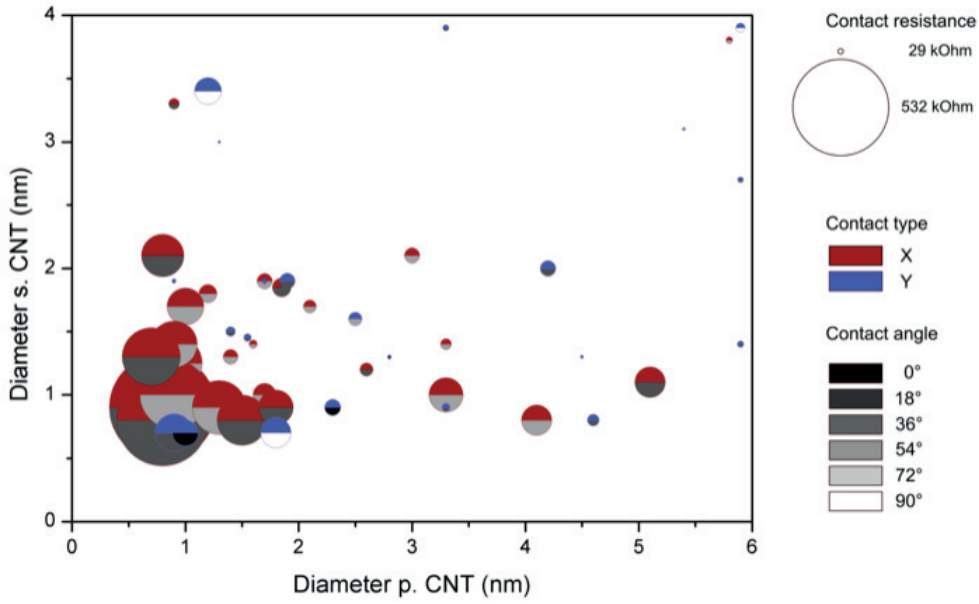

Figure 5.8. Contact resistance of X and Y junctions vs. diameters of primary (p.) and secondary (s.) SWCNTs and their intersecting angles. Y-junctions had smaller resistances than X-junctions at any given structural parameter with minimum value of 29 kΩ. The contact resistance reduced with increasing SWCNT or bundle diameters of the contacting branches (Publication 3).

To study the effect of the nitric acid treatment, samples were prepared by dipping SWCNT-N films into nitric acid (Sigma Aldrich, 68% HNO_3). A comparison between the contact resistances of X-contacts before and after treatment is shown in Figure 5.9. b). The average contact resistance was reduced by a factor of ~ 3 after nitric acid treatment. The comparison was carried out for X-contacts with diameter > 1 nm, with 28 characterised contacts before and 9 after the chemical treatment. We also measured the resistance per unit length before and after the treatment for a number of SWCNTs as shown in Figure 5.8. c). No significant change of resistance per unit length was observed through the treatment.

The results show that chemical treatment is mainly lowering the contact resistance between SWCNTs as covalent reactions on SWCNT walls should lead to increased resistance along SWCNT length. Charge transfer without covalent reactions has been suggested in several papers [97], [98], [99]. This agrees with Raman-analysis of pristine and doped SWCNT-Ns which showed that the G/D ratio remains largely unchanged after the treatment. Therefore, we conclude that a rapid acid treatment improves the overall conductivity of SWCNT networks by lowering the contact resistances without introducing a significant number of structural defects such as covalently bonded functional groups, which would increase the resistance per unit length of SWCNTs. The electrical transport measurement obtained for ethanol-densified films exhibited a sheet resistance of about 400 Ω/sq. at 80% transmittance. The chemically treated films showed an improved performance with the sheet resistance decreasing to 100 Ω/sq. at 80% transmittance, which corresponds to a reduction by a factor of 4.

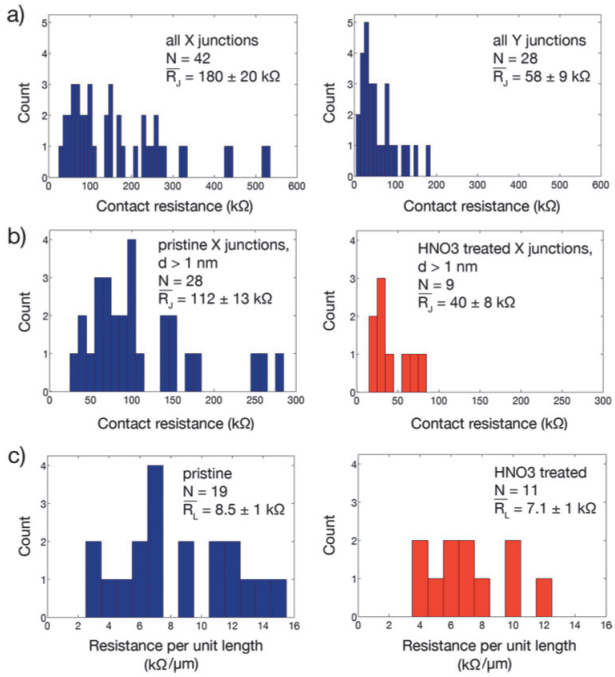

Figure 5.9. a) The overall contact resistance of X-type and Y-type contacts show that the Y-type contacts had lower contact resistance compared to X-type contacts. b) The X-type contacts for d > 1 nm tubes and bundles showed a significant reduction in sheet resistance after HNO_3 treatment. c) However, the resistance per unit length was only slightly reduced (Publication 3).

5.4 Novel-Room Temperature Press Transfer Technique

Aerosol-CVD synthesis, when combined with filtration can be used to fabricate tuneable thickness SWCNT networks. Indeed, SWCNT networks consisting of shorter bundles were previously transferred to flexible PE-substrates by using the thermo-compression technique, which relies on heating of the substrate material to temperatures within the range of 90 °C to 130 °C [80]. In this work (Publication 1) the press-transfer process was shown to work at ambient conditions around 20 °C without additional heating. Nitrocellulose filters were used for SWCNT-network collection. In order to transfer a network to a substrate, a moderate pressure of approximately 1 kPa was applied by metal plates to contact the SWCNT network and substrate for around 15 s. After the pressing process the membrane filter can be peeled off and the SWCNT-N stays adhered to the receiving substrate. Interestingly, no additional dispersion or purification steps are needed, and the SWCNT-networks can be used without any additional treatments. SWCNT-Ns up to 28 cm x 28 cm were successfully fabricated. The transfer process is fast and manual transfer can be achieved in less than 15 s whilst the duration can be further reduced by automatisation. A typical manually performed press-transfer process of SWCNT-N is depicted in Figure 5.10.

Figure 5.10. A typical manually performed room-temperature press transfer process. A filter with aerosol-CVD synthesised SWCNT network was placed on a substrate material, which was in this case a transparent PET-film. The SWCNT-network and the substrate were pressed together with moderate pressure around 1 kPa, by using a flat metal disk at room-temperature. Following this, the membrane filter was peeled of and the SWCNT films stays adhered to the substrate (Publication 1).

Furthermore, by pre-patterning a non-gas permeable mask to the filter surface, localised deposition patterns can be achieved. The technique can also used be with a wide range of substrates from flexible polymers (PET, PE, PEN) to glass, quartz, silicon and silicon dioxide, as well as various metals, thus further increasing the flexibility of the process, as clearly demonstrated in Figure 5.11. Further deposition size scaling is also straightforward, and can be achieved by simply increasing the size of the filtration membrane. The room-temperature press transfer is also compatible with roll-to-roll processing techniques, thus increasing the industrialisation potential for this technique.

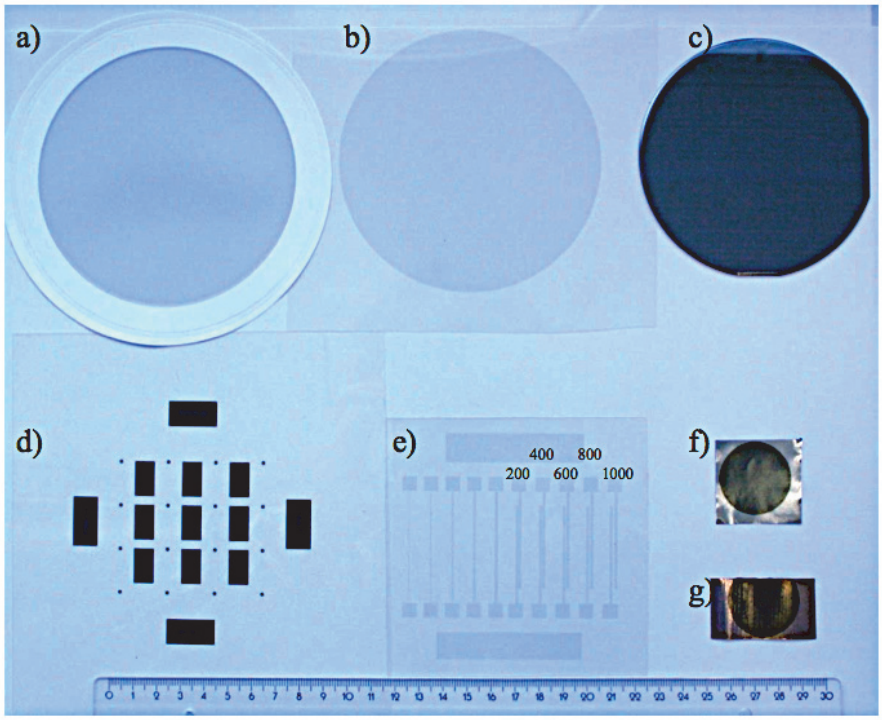

Figure 5.11. The room-temperature press transfer technique is compatible with wide range of substrates. This image depicts various substrates with dry transferred SWCNT-networks: a) a filter covered by SWCNTs after filtering the flow at the outlet of the reactor; b) SWCNT-network film on PET; c) a silicon wafer fully covered by SWCNT-network; d) and e) SWCNT-networks patterned using masks under the filter and transferred to PET. The number shows the distance between electrodes in micrometers. SWCNT-network on f) Fe and g) Cu foils (Publication 1).

The application potential of the SWCNT TCFs fabricated with the room-temperature press transfer process was demonstrated by fabricating various devices. For example, the SWCNT TCF was used as the transparent conductive electrode for capacitive touch sensing application. A highly transparent SWCNT network (98%, sheet resistance 4 kΩ/sq.) was transferred to a PET substrate, which was connected to a PCB with read-out electronics based on commercially available touch sensor chipset and touch indicator led (QT100, Atmel Corporation). When compared to a reference device with a copper touch sensor electrode the SWCNT network exhibited similar touch sensitivity as the metal electrodes, while offering complete transparency. Interestingly, the SWCNT can be connected with commercial silver paint with low contact resistance of around 50 Ω. The touch sensor demonstrator device and the schematics for the read-out electronics used for capacitive touch detection are shown in Figure 5.12.

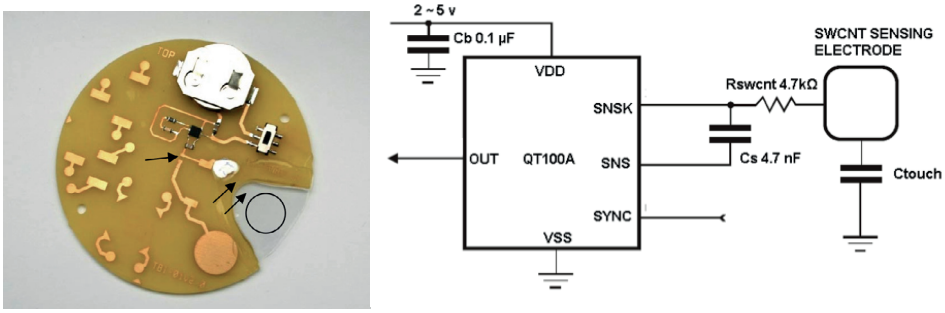

Figure 5.12. SWCNT thin film can be used as transparent conductive film for capacitive touch sensing as the transparent sensor electrode, with simple, commercially available read-out electronics (Publication 1).

To summarise, single-walled carbon nanotubes have major potential for a wide range of transparent conducting film applications. SWCNTs can offer high optical transparency, competitive electrical performance with ITO-on-polymer and improved flexibility, thus making SWCNT TCFs ideal for potential utilisation in conjunction with high volume roll-to-roll manufacturing methods. Additionally, the carbon nanotubes have several unique properties, which enable applications beyond simple ohmic TCFs such as utilisation of the semi-conductive thin SWCNT networks as TFT-channels.

SWCNTs can be synthesised by using commonly available materials including iron as catalyst particles and carbon precursors, thus reducing the supply and price risks of the traditional TCF materials. The current industry relies on availability of indium, and its production and exports are tightly controlled by China. Indeed, it has recently been the subject of aggressive trade policies. SWCNT-TCFs and several other alternative TCF materials have been developed during recent years, each offering varying combinations of optoelectrical performance, ease of manufacturing, environmental stability and cost of materials. In the long run, successful alternative TCF materials for applications will be selected through a combination of these parameters. As the adaptation of new materials and production technologies requires typically capital intensive investments to new production equipment and R&D, the commercial competitive advantage must be significant to create widespread market acceptance.

5.5 Multifunctional Free-standing SWCNT films

We found that the room-temperature press transfer process can also be used for the fabrication of novel, free-standing, large-area SWCNT networks (Publication 2). The substrates were perforated prior to the deposition process, whilst the substrate material was used only as a supporting frame to ease the handling of the free-standing SWCNT networks and to help maintain the flat structure. The free-standing film (FSF) transfer process is fast and compatible a with wide range of frame materials, including flexible polymers, glass, quartz, silicon and various metals. It also allows for the fabrication of large area freestanding films up 70 mm in diameter of the freestanding area. A few examples of freestanding SWCNT films are presented in Figure 5.13. The substrate-free nature of the free-standing network allows for the realisation of many novel applications, where the substrate is not allowed such as gas filtration, heating and thermoacoustic emission, all of which are discussed in more detail in the original publication.

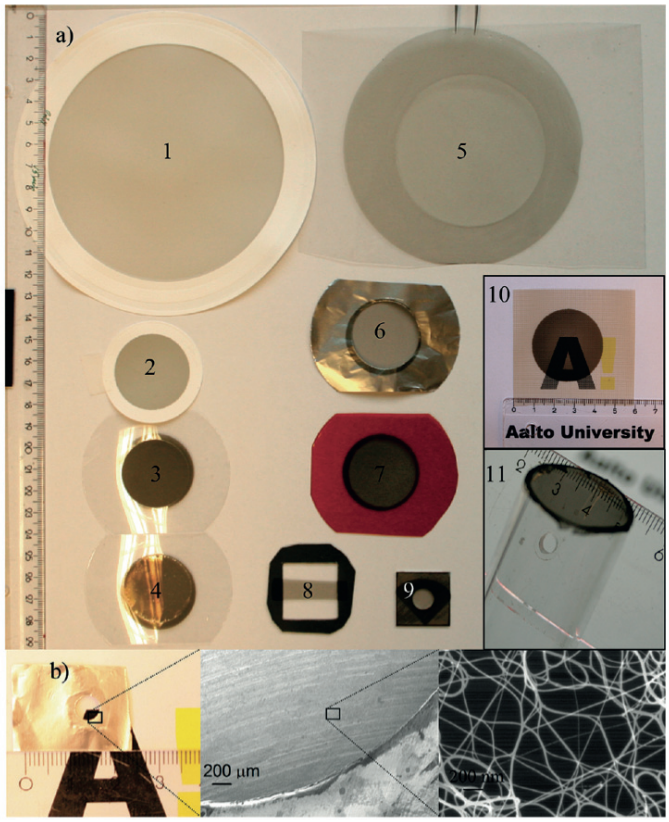

Figure 5.13. Novel, large area freestanding films (FSF) supported by various substrate materials. a) Photograph of nitrocellulose filters with collected SWCNT films (1,2), pristine and ethanol-densified films suspended over 30 mm openings in PET (3 and 4, respectively), FSF on PET over 70 mm hole (5), FSF on aluminium foil (6), FSF on Kapton (7), a strip of FSF suspended over a rectangular hole in a plastic sheet (8), and FSF on cold rolled steel (9). The inset shows (10) a semi-free-standing film on a polyetherketone substrate with 120 µm diameter holes (with an open area of 49%) and (11) an FSF suspended over the open end of a glass tube of internal diameter 20 mm. b) Set of images showing a sub-monolayer FSF suspended over 5 mm openings in aluminium foil (Publication 2).

5.6 SWCNT Electrodes for Dye-sensitised Solar Cells

SWCNT films were studied as DSC counter-electrode material (Publication 4). The goal was to use the flexibility, electrical conductivity and catalytic activity of the SWCNT networks towards the tri-iodide reduction reaction in counter-electrode of a DSC. When compared to the traditional counter-electrode materials such as platinum thin films, the SWCNTs offer greatly enhanced flexibility and if the optoelectrical performance is good enough, partial transparency allows for cell illumination both from photo-electrode and counter-electrode sides.

To improve the catalytic performance of SWCNT network counter electrodes, the utilisation of PEDOT was studied (Publication 4). Conductive PEDOT was electro-polymerised on SWCNT network on PET-substrate. The counter-electrode performance between the SWCNT, the PEDOT-SWCNT and the thermally deposited and sputtered platinum counter-electrodes was compared. The results indicated that the PEDOT-SWCNT counter-electrodes exhibit energy conversion efficiency of 4%, whereas the SWCNT films had an efficiency of 2%. The reference counter-electrodes exhibited efficiencies of around 4%, and more specifically 3.9% for sputtered Pt on ITO-PET and 4.3% for the thermally deposited Pt on FTO-glass. Moreover, the fill factors were significantly enhanced when compared to single component SWCNT films as indicated in Table 5.14. and Figure 5.15. The improved performance due to the PEDOT deposition was explained by lowered charge transfer resistance, while the series resistance was found to be at comparable levels by using electrostatic impedance spectroscopy (EIS).

Table 5.14. Summary of the electrical properties and DSC performance of cells with various counter-electrode materials (Publication 4).

CE type	R_s (Ω/sq.)	T (%)	# of cells	i_{SC} (mA/cm^2)	V_{OC} (V)	F.F. (%)	Efficiency (%)
PEDOT–SWCNT	12.2 ± 0.4	5 ± 1	6	11 ± 0.4	0.58 ± 0.01	63 ± 2	4.0 ± 0.1
SWCNT	11.8 ± 0.4	10 ± 1	4	12 ± 0.2	0.61 ± 0.01	28 ± 1	2.0 ± 0.1
Sputtered Pt-ITO–PET	23 ± 0.7	21 ± 1	4	14 ± 0.5	0.59 ± 0.01	46 ± 2	3.9 ± 0.2

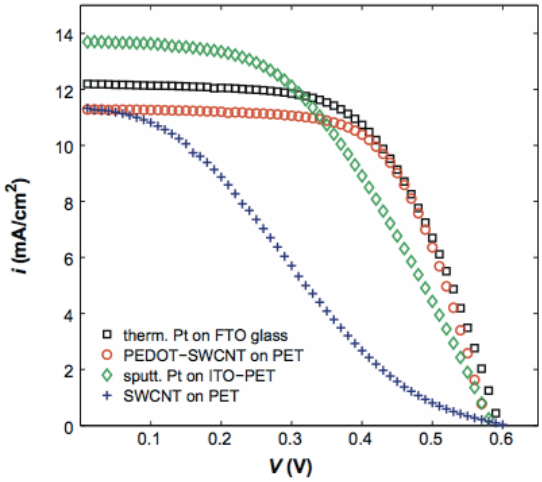

Figure 5.15. The IV-curves for DSC with different counter-electrode types (Publication 4).

5.7 Carbon Coating of SWCNT Networks

The utilisation of carbon coatings to improve the mechanical durability of SWCNT networks was studied as one part of this research (Publication 5). Formation of the coating was observed first by comparing SEM-micrographs of the ethanol densified non-coated and carbon PVD-coated networks as indicated in Figure 5.16. The figure depicts the network surface morphology prior to and following 250 PVD-coating pulses, which form an approximately 25 nm thick coating. The imaging revealed that the carbon coating significantly modifies the SWCNT network surface layers, thickening the bundles and partially covering the pores in the network, while the basic interconnected network morphology is maintained. Heavy mechanical scratching of the coated networks revealed that the structural modification due to the carbon-PVD process is localised to the surface layers of the network, while the underlying layers are shadowed by the top layers.

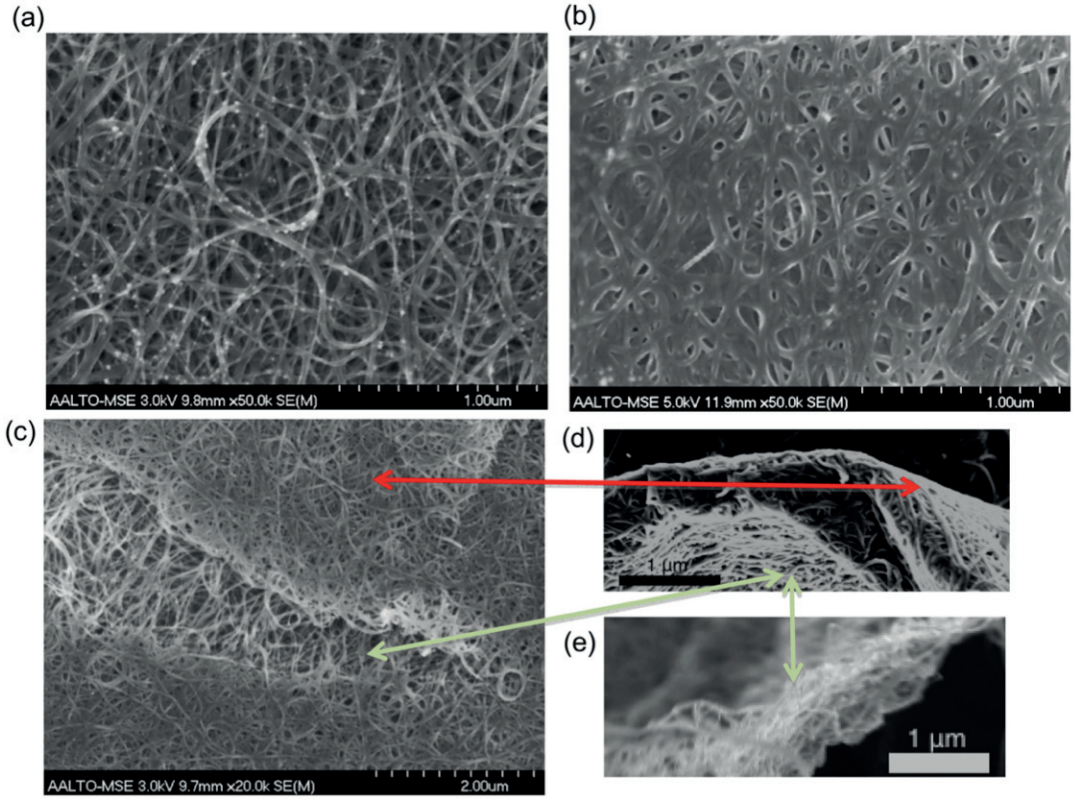

Figure 5.16. SEM images of a) an ethanol densified SWCNT network and b) an ethanol densified, PVD-coated SWCNT hybrid nanomaterial c) a macroscopic scratch, which reveals a crust-like, highly interconnected, coating modified SWCNT network near the top-surface of the sample, and underlying pristine SWCNT-network, d) a cross sectional view of the PVD-coated network (indicated by the red arrow) and e) the non-coated densified SWCNT-network (indicated by green arrows), showing the effects of carbon coating to the morphology of the SWCNT network (Publication 5).

The sheet resistance was characterised for PVD-coated samples both *in-situ* during the coating process and *ex-post* after removing the samples from the vacuum level deposition chamber. The in-situ measurement performed after individual coating pulses revealed a rapid increase in the sheet resistance values during the first few pulses, although the increase was rapidly stabilised to constant value, while the thin SWCNT network still maintained reasonable electrical conductivity. Interestingly, the sheet resistance rapidly recovered when the sample was removed from the vacuum coating chamber, thus indicating that the increase in the sheet resistance is at least partially explained by the removal of ambient species such as oxygen and water on the bundle surfaces (Figure 5.17). Thicker, densified SWCNT TCFs were also evaluated and revealed a significantly smaller sheet resistance increase from 100 Ω/sq. to 220 Ω/sq. while the optical transparency was reduced from 50% to 40%, respectively.

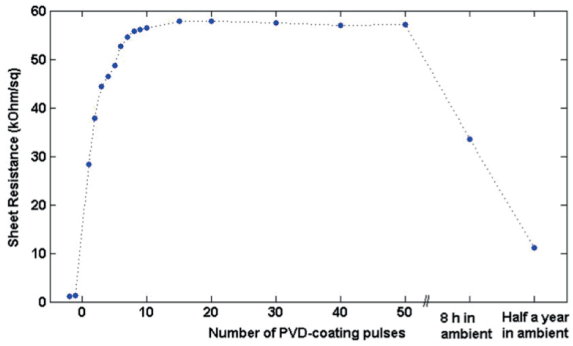

Figure 5.17. *In-situ* measurement of a thin, highly transparent SWCNT network sheet resistance during the PVD carbon coating process. The increase in sheet resistance stabilised after 10 pulses and recovered significantly after the sample was exposed to ambient conditions (Publication 5).

The carbon plasma coating was shown to improve the mechanical durability of the SWCNT networks under nanoindentation and nanowear testing. The pristine and coated films were first tested by performing three concentric nanowear scans starting from size 15 x 15 μm², 10 x 10 μm² and 5 x 5 μm², with increasing loadings of 1 μN, 10 μN and 25 μN respectively. For the non-coated networks all the scan areas are clearly visible in the post-wear SEM imaging and the whole surface is roughened when compared to non-worn areas as indicated in Figure 5.18. The network is deformed already by the smallest loading of 1 μN and SWCNTs were largely removed when the load was increased to 25 μN. The carbon plasma coated SWCNT network maintained its integrity much better, and only the highest loading condition area was clearly visible in the post-wear SEM and SPM-scans, indicating the improved nanomechanical durability of the carbon plasma coated SWCNT films, when compared to their pristine counterparts.

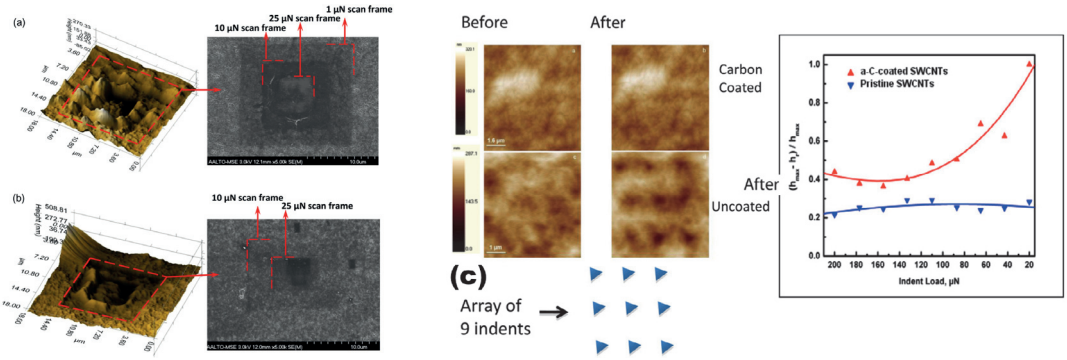

Figure 5.18. Scanning probe microscopy and scanning electron microscopy images of worn a) non-coated and b) carbon coated SWCNT networks by scan-wear tests at different loads. The coated network was more resilient and wear resistant than the non-coated one. c) SPM images before and after indentation on the coated SWCNT network, and on the non-coated network. There were hardly any observable changes after the indentation on the surface of the coated networks. However, the 9 indent marks were clearly visible on the non-coated network surface, which was also evident in the ratio of indentation depth recovery at each peak-load (Publication 5).

The nano-indentation load-displacement curves also supported the improved resiliency of carbon coated SWCNT networks as indicated by the SPM scans and recovered indentation depths, which are shown in Figure 5.16. c). The peak load was chosen to be low enough to ensure the minimal substrate interaction and to avoid complete penetration of the SWCNT network, to focus on the response of the network. The carbon plasma coated network demonstrated higher resistance to the indentation and larger elastic recovery. The ratio of the recovered depth to the maximum penetration depth as calculated by the equation $(h_{max} - h_t)/h_{max}$, where h_{max} is the corresponding depth at the maximum load and h_t is the residual depth. The SPM scans performed post-loading revealed no-detectable indentation marks on the coated sample surface, while the non-coated SWCNT networks had permanent indentation marks. The SWCNT bundles were easily movable by the SPM tip and the carbon coating reduced the amount of permanent deformation and improved the strength of the networks both under nanoindentation and nanowear conditions.

6 Conclusions

This thesis investigated aerosol-CVD synthesised SWCNTs, with a focus on their transparent conductive film applications. The synthesis conditions and reactor configuration were optimised for high conductivity SWCNT-N TCFs. In parallel, a rapid chemical post-deposition treatment was developed. When combined, these developments resulted in a significant performance improvement as the sheet resistance was reduced over two orders of magnitude from 22 kΩ/sq. to 84 Ω/sq. at 90% transparency, thus making the SWCNT thin film transparent films competitive with industry standard ITO on flexible polymers and among the best values for carbon nanomaterial based TCFs. The mechanism for sheet resistance improvement was explained by a SWCNT bundle length increase from 1.3 μm to 9.4 μm. This was achieved through growth condition optimisation and reactor scaling as observed from pristine, low density samples. The bundle diameter distributions were overlapping, with mean bundle diameter of around 10 nm, while mean SWCNT diameters ranged from 1.4 to 1.7 nm. The TEM-analysis carried out for the sample collected from the same synthesis condition suggested that the majority of SWCNTs have high chiral angles close to armchair edge. The increased bundle length led to a reduction in highly resistive bundle-bundle contacts, which has a major impact on the overall resistance of SWCNT networks.

C-AFM measurements of pristine and acid treated SWCNTs were performed in order to estimate their resistances per unit length and contact resistances between bundles. The contact resistance values of pristine junctions were in the range of 29 kΩ - 532 kΩ for a sample consisting dominantly of contacts between individual tubes small bundles with smaller than 5 nm diameter. High contact angle i.e. X-type contacts were found to exhibit higher mean contact resistance of 180 kΩ whereas low contact angle i.e. Y-type contacts had mean contact resistance of 60 kΩ. The diameters of connected SWCNTs or SWCNT-bundles were observed to have a dominant role in determining the overall contact resistance, whilst the contact resistance was reduced with increasing bundle diameter. The contact resistances were reduced by a factor of ~ 3 after nitric acid treatment, although the length resistivity remained largely unchanged at around 8 kΩ/μm. The nitric acid treatment had no significant effect on the resistance per unit length, thus suggesting that the

performance improvement was due to reduction of the contact resistances. The results indicate that the contact morphology and diameter of contacting SWCNTs and bundles have a significant impact on the electrical transport across the contacts and that the nitric acid treatment mainly affects the network performance by modulating the contacts and reducing their contact resistances. This conclusion is also supported by the results of acid treatment of SWCNT networks consisting of different bundle lengths, where the acid treatment had the largest effect (13x) on the sample comprising short bundles of 1.3 μm. Indeed, in SWCNT networks consisting of longer bundles of 9.4 μm the acid treatment reduction was only 5x on average.

The room-temperature press transfer technique was developed to enable the rapid and straightforward deposition of aerosol-CVD synthesised SWCNT networks, with tuneable thickness, transparency and sheet resistance to a wide range of substrates. The dry deposition method eliminates the need for pre-deposition liquid treatments and thus helps to maintain the high intrinsic quality of the aerosol-CVD synthesised SWCNTs. The deposition process is significantly faster and less resource consuming than conventional SWCNT dispersion, purification and network formation methods. The developed room-temperature deposition method has already been adopted for industrial production by Canatu Ltd. who are utilising it for Carbon NanoBud based touch sensor production at their medium-scale production facilities in Helsinki, Finland. Several other companies from different countries are working to commercialise CNT-based touch sensors or TCFs. This suggests that the cost structure of the CNT-based TCFs is favourable for commercial production, even though presenting and discussing the detailed manufacturing cost estimates is outside the scope of this thesis.

Furthermore, the developed press transfer technique was used to fabricate novel, freestanding SWCNT networks, which offer a wide range of novel applications for thin, transparent and conductive SWCNT films. The SWCNT networks and the developed processing techniques were applied to the fabrication of flexible counter-electrodes for dye-sensitised solar cells. The SWCNT networks were demonstrated as a combined catalyst and partially transparent electrode providing flexibility and potential roll-to-roll processing compatibility. The flexible PEDOT decorated SWCNT-network counter-electrodes reached comparable performance with rigid, platinum coated ITO-glass based counter electrodes, with energy conversion efficiencies up to 4%. Also studied were the fabrication and properties of hybrid material consisting of SWCNT network modified by carbon coating. The coating improved the mechanical durability of SWCNT films under nanoindentation and scratching, while the electrical conductivity and optical transparency characteristics of the hybrid material were largely maintained.

For future research the continuing improvement of the optoelectrical performance remains as a key issue. This could be achieved by further optimising the SWCNT growth process, so as to reduce the number of bundle-bundle contacts by synthesising longer, defect-free tubes with long charge carrier mean free path. Indeed, this should lead to improved electrical performance. Reducing bundling of SWCNT-Ns either by aerosol concentration control during the synthesis or by electrostatic filtration of the charged bundles at the outlet of the reactor are interesting when it comes to the fabrication of SWCNT-Ns with a high number of individual SWCNTs. These networks

should have a higher number of parallel conduction paths at the same optical transparency and thus higher optoelectrical performance when compared to bundled SWCNT-N TCFs. Other approaches, such as aligned SWCNT-Ns or more effective treatment agents should also be studied as potential ways in which to achieve additional resistance reduction. Moreover, the development of direct deposition of SWCNTs from the gas phase to substrate would further simplify the fabrication process and completely eliminate the potential contamination by liquid treatment. Furthermore, the developed synthesis and processing techniques can be used for fabrication of SWCNT-N based thin film transistors, which is a very interesting research direction and could lead to the development of active SWCNT based devices. However, the transistor applications require an even higher degree of control over the properties of SWCNTs whilst the metallicity, diameter, length and bundling control are even more important than for TCFs.

7 References

[1]Z. Wu, “Transparent, Conductive Carbon Nanotube Films,” *Science*, vol. 305, no. 5688, pp. 1273–1276, Aug. 2004.

[2]Q. Cao and J. A. Rogers, “Ultrathin Films of Single-Walled Carbon Nanotubes for Electronics and Sensors: A Review of Fundamental and Applied Aspects,” *Adv. Mater.*, vol. 21, no. 1, pp. 29–53, Jan. 2009.

[3]H. Park, A. Afzali, S.-J. Han, G. S. Tulevski, A. D. Franklin, J. Tersoff, J. B. Hannon, and W. Haensch, “High-density integration of carbon nanotubes via chemical self-assembly,” *Nature Nanotech*, vol. 7, no. 12, pp. 787–791, Oct. 2012.

[4]Solid State Technology, “ITO alternatives infiltrating transparent conductive films market,” pp. 1–4, 21-Feb.-2013.

[5]Displayback Co. Ltd., *2011 Touch Panel - Use of ITO Film/ITO Glass*, vol. 2010. 2010, pp. 1–163.

[6]L. Ke, R. S. Kumar, S. J. Chua, and A. P. Burden, “Degradation study in flexible substrate organic light-emitting diodes,” *Appl. Phys. A*, vol. 81, no. 5, pp. 969–974, Jan. 2005.

[7]M. Segal, “Selling graphene by the ton,” *Nature Nanotech*, vol. 4, no. 10, pp. 612–614, Oct. 2009.

[8]M. Humphries, *Rare earth elements: The global supply chain*, vol. 2010. DIANE Publishing, 2013.

[9]“File:Eight Allotropes of Carbon.png - Wikipedia, the free encyclopedia,” *enwikipediaorg*. [Online]. Available: http://en.wikipedia.org/wiki/File:Eight_Allotropes_of_Carbon.png. [Accessed: 21-Aug.-2013].

[10]S. Iijima and T. Ichihashi, “Single-shell carbon nanotubes of 1-nm diameter,” *Nature*, vol. 363, no. 17, pp. 1–3, Jun. 1993.

[11]D. S. Bethune, C. H. Kiang, M. S. de Vries, G. Gorman, R. Savoy, J. Vazquez, and R. Beyers, “Cobalt-catalyzed growth of carbon nanotubes with single-atomic-layer walls,” *Nature*, vol. 363, no. 17, pp. 1–3, Jun. 1993.

[12]K. S. Novoselov, “Electric Field Effect in Atomically Thin Carbon Films,” *Science*, vol. 306, no. 5696, pp. 666–669, Oct. 2004.

[13]“File:CNTnames.png - Wikimedia Commons,” *commons.wikimedia.org*. [Online]. Available: http://commons.wikimedia.org/wiki/File:CNTnames.png.[Accessed: 21-Aug.-2013].

[14]Y. Ando, X. Zhao, T. Sugai, and M. Kumar, “Growing carbon nanotubes,” *Materials today*, vol. 7, no. 10, pp. 22–29, 2004.

[15]C. D. Scott, S. Arepalli, P. Nikolaev, and R. E. Smalley, “Growth mechanisms for single-wall carbon nanotubes in a laser-ablation process,” *Appl. Phys. A*, vol. 72, no. 5, pp. 573–580, May 2001.

[16]N. Grobert, “Carbon nanotubes–becoming clean,” *Materials today*, vol. 10, no. 1, pp. 28–35, 2007.

[17]P. R. Mudimela, A. G. Nasibulin, H. Jiang, T. Susi, D. Chassaing, and E. I. Kauppinen, “Incremental Variation in the Number of Carbon Nanotube Walls with Growth Temperature,” *J. Phys. Chem. C*, vol. 113, no. 6, pp. 2212–2218, Feb. 2009.

[18]S. M. Bachilo, L. Balzano, J. E. Herrera, F. Pompeo, D. E. Resasco, and R. B. Weisman, “Narrow (n, m)-Distribution of Single-Walled Carbon Nanotubes Grown Using a Solid Supported Catalyst,” *J. Am. Chem. Soc.*, vol. 125, no. 37, pp. 11186–11187, Sep. 2003.

[19]H. M. Cheng, F. Li, X. Sun, S. Brown, M. A. Pimenta, A. Marucci, G. Dresselhaus, and M. S. Dresselhaus, “Bulk morphology and diameter distribution of single-walled carbon nanotubes synthesized by catalytic decomposition of hydrocarbons,” *Chemical Physics Letters*, vol. 289, no. 5, pp. 602–610, 1998.

[20]A. Moisala, A. G. Nasibulin, D. P. Brown, H. Jiang, L. Khriachtchev, and E. I. Kauppinen, “Single-walled carbon nanotube synthesis using ferrocene and iron pentacarbonyl in a laminar flow reactor,” *Chemical Engineering Science*, vol. 61, no. 13, pp. 4393–4402, Jul. 2006.

[21]Z. Zhou, L. Ci, L. Song, X. Yan, D. Liu, H. Yuan, Y. Gao, J. Wang, L. Liu, and W. Zhou, “Producing cleaner double-walled carbon nanotubes in a floating catalyst system,” *Carbon*, vol. 41, no. 13, pp. 2607–2611, 2003.

[22]B. Zhang, G. Hong, B. Peng, J. Zhang, W. Choi, J. M. Kim, J.-Y. Choi, and Z. Liu, “Grow Single-Walled Carbon Nanotubes Cross-Bar in One Batch,” *J. Phys. Chem. C*, vol. 113, no. 14, pp. 5341–5344, Apr. 2009.

[23]G. Gruner, “Carbon nanotube films for transparent and plastic electronics,” *J. Mater. Chem.*, vol. 16, no. 35, p. 3533, 2006.

[24]M. Kaempgen, G. S. Duesberg, and S. Roth, “Transparent carbon nanotube coatings,” *Applied Surface Science*, vol. 252, no. 2, pp. 425–429, Oct. 2005.

[25]T. V. Sreekumar, T. Liu, S. Kumar, L. M. Ericson, R. H. Hauge, and R. E. Smalley, “Single-Wall Carbon Nanotube Films,” *Chem. Mater.*, vol. 15, no. 1, pp. 175–178, Jan. 2003.

[26]J.-H. Shin, D. W. Shin, S. P. Patole, J. H. Lee, S. M. Park, and J. B. Yoo, “Smooth, transparent, conducting and flexible SWCNT films by filtration–wet transfer processes,” *J. Phys. D: Appl. Phys.*, vol. 42, no. 4, p. 045305, Jan. 2009.

[27]N. Hamada, S.-I. Sawada, and A. Oshiyama, “New one-dimensional conductors: Graphitic microtubules,” *Physical Review Letters*, pp. 1–3, Mar. 1992.

[28]“File:Band structure CNT.jpg - Wikipedia, the free encyclopedia,” *enwikipediaorg*. [Online]. Available: http://en.wikipedia.org/wiki/File:Band_structure_CNT.jpg. [Accessed: 21-Aug.-2013].

[29]H. Kataura, Y. Kumazawa, Y. Maniwa, I. Umezu, S. Suzuki, Y. Ohtsuka, and Y. Achiba, “Optical properties of single-wall carbon nanotubes,” *Synthetic Metals*, vol. 103, no. 1, pp. 2555–2558, 1999.

[30]Y. Tian, “Optical Properties of Single-walled Carbon Nanotubes and Nanobuds,” Aalto University, 2012.

[31]L. Hu, D. S. Hecht, and G. Grüner, “Carbon Nanotube Thin Films: Fabrication, Properties, and Applications,” *Chem. Rev.*, vol. 110, no. 10, pp. 5790–5844, Oct. 2010.

[32]"File:SSPN41.PNG - Wikipedia, the free encyclopedia," *enwikipediaorg*. [Online]. Available: http://en.wikipedia.org/wiki/File:SSPN41.PNG.[Accessed: 21-Aug.-2013].

[33]C. Fantini, A. Jorio, M. Souza, M. Strano, M. Dresselhaus, and M. Pimenta, "Optical Transition Energies for Carbon Nanotubes from Resonant Raman Spectroscopy: Environment and Temperature Effects," *Physical Review Letters*, vol. 93, no. 14, p. 147406, Sep. 2004.

[34]M. S. Dresselhaus, G. Dresselhaus, R. Saito, and A. Jorio, "Raman spectroscopy of carbon nanotubes," *Physics Reports*, vol. 409, no. 2, pp. 47–99, Mar. 2005.

[35]D.-M. Sun, M. Y. Timmermans, Y. Tian, A. G. Nasibulin, E. I. Kauppinen, S. Kishimoto, T. Mizutani, and Y. Ohno, "Flexible high-performance carbon nanotube integrated circuits," pp. 1–6, Feb. 2011.

[36]M. S. Fuhrer, J. Nygård, L. Shih, M. Forero, Y.-G. Yoon, H. J. Choi, J. Ihm, S. G. Louie, A. Zettl, and P. L. McEuen, "Crossed nanotube junctions," *Science*, vol. 288, no. 5465, pp. 494–497, 2000.

[37]A. Javey, J. Guo, M. Paulsson, Q. Wang, D. Mann, M. Lundstrom, and H. Dai, "High-Field Quasiballistic Transport in Short Carbon Nanotubes," *Physical Review Letters*, vol. 92, no. 10, p. 106804, Mar. 2004.

[38]S. Li, Z. Yu, C. Rutherglen, and P. J. Burke, "Electrical Properties of 0.4 cm Long Single-Walled Carbon Nanotubes," *Nano Lett.*, vol. 4, no. 10, pp. 2003–2007, Oct. 2004.

[39]D. Hecht, L. Hu, and G. Grüner, "Conductivity scaling with bundle length and diameter in single walled carbon nanotube networks," *Appl. Phys. Lett.*, vol. 89, no. 13, p. 133112, 2006.

[40]P. N. Nirmalraj, P. E. Lyons, S. De, J. N. Coleman, and J. J. Boland, "Electrical Connectivity in Single-Walled Carbon Nanotube Networks," *Nano Lett.*, vol. 9, no. 11, pp. 3890–3895, Nov. 2009.

[41]C. Donnet and A. Erdemir, *Tribology of diamond-like carbon films*. USA: Springer, 2008, pp. 1–1.

[42]J. Robertson, "Diamond-like amorphous carbon," *Materials Science and Engineering: R: Reports*, vol. 37, no. 4, pp. 129–281, 2002.

[43]H. Kinoshita, I. Ippei, H. Sakai, and N. Ohmae, "Synthesis and mechanical properties of carbon nanotube/diamond-like carbon composite films," *Diamond & Related Materials*, vol. 16, no. 11, pp. 1940–1944, Nov. 2007.

[44]C. Wei, C.-I. Wang, F.-C. Tai, K. Ting, and R.-C. Chang, "The effect of CNT content on the surface and mechanical properties of CNTs doped diamond like carbon films," *Diamond & Related Materials*, vol. 19, no. 5, pp. 562–566, May 2010.

[45]H. Schittenhelm, D. B. Geohegan, G. E. Jellison, A. A. Puretzky, M. J. Lance, and P. F. Britt, "Synthesis and characterization of single-wall carbon nanotube–amorphous diamond thin-film composites," *Appl. Phys. Lett.*, vol. 81, no. 11, p. 2097, 2002.

[46]D.-H. Kim, M.-R. Park, H.-J. Lee, and G.-H. Lee, "Thickness dependence of electrical properties of ITO film deposited on a plastic substrate by RF magnetron sputtering," *Applied Surface Science*, vol. 253, no. 2, pp. 409–411, Nov. 2006.

[47]L. Kerkache, A. Layadi, E. Dogheche, and D. Rémiens, "Physical properties of RF sputtered ITO thin films and annealing effect," *J. Phys. D: Appl. Phys.*, vol. 39, no. 1, pp. 184–189, Dec. 2005.

[48]R. A. Synowicki, “Spectroscopic ellipsometry characterization of indium tin oxide film microstructure and optical constants,” *Thin Solid Films*, vol. 313, pp. 394–397, 1998.

[49]K. Salazar and M. K. McNutt, “MINERAL COMMODITY SUMMARIES 2012,” U.S. Department of the Interior and U.S. Geological Survey, Jan. 2013.

[50]“Metal Bulletin - 99,99% Indium ingots,” http://www.metalbulletin.com/Article/3102461/Minor-and-precious-metals/, 26-Feb.-2013.

[51]Dolcera, “LCD Technologies,” *Dolcera.com*, 26-Feb.-2013. [Online]. Available: http://www.dolcera.com/wiki/index.php?title=LCD_Technologies. [Accessed: 26-Feb.-2013].

[52]H.-Z. Geng, K. K. Kim, K. P. So, Y. S. Lee, Y. Chang, and Y. H. Lee, “Effect of Acid Treatment on Carbon Nanotube-Based Flexible Transparent Conducting Films,” *J. Am. Chem. Soc.*, vol. 129, no. 25, pp. 7758–7759, Jun. 2007.

[53]B. B. Parekh, G. Fanchini, G. Eda, and M. Chhowalla, “Improved conductivity of transparent single-wall carbon nanotube thin films via stable postdeposition functionalization,” *Appl. Phys. Lett.*, vol. 90, no. 12, p. 121913, 2007.

[54]A. A. Green and M. C. Hersam, “Colored Semitransparent Conductive Coatings Consisting of Monodisperse Metallic Single-Walled Carbon Nanotubes,” *Nano Lett.*, vol. 8, no. 5, pp. 1417–1422, May 2008.

[55]A. A. Green and M. C. Hersam, “Processing and properties of highly enriched double-wall carbon nanotubes,” *Nature Nanotech*, vol. 4, no. 1, pp. 64–70, Dec. 2008.

[56]E. M. Doherty, S. De, P. E. Lyons, A. Shmeliov, P. N. Nirmalraj, V. Scardaci, J. Joimel, W. J. Blau, J. J. Boland, and J. N. Coleman, “The spatial uniformity and electromechanical stability of transparent, conductive films of single walled nanotubes,” *Carbon*, vol. 47, no. 10, pp. 2466–2473, Aug. 2009.

[57]B. Dan, G. C. Irvin, and M. Pasquali, “Continuous and Scalable Fabrication of Transparent Conducting Carbon Nanotube Films,” *ACS Nano*, vol. 3, no. 4, pp. 835–843, Apr. 2009.

[58]“Graphene, a promising transparent conductor,” pp. 1–8, Jan. 2013.

[59]C. Mattevi, G. Eda, S. Agnoli, S. Miller, K. A. Mkhoyan, O. Celik, D. Mastrogiovanni, G. Granozzi, E. Garfunkel, and M. Chhowalla, “Evolution of Electrical, Chemical, and Structural Properties of Transparent and Conducting Chemically Derived Graphene Thin Films,” *Adv. Funct. Mater.*, vol. 19, no. 16, pp. 2577–2583, Aug. 2009.

[60]A. Reina, X. Jia, J. Ho, D. Nezich, H. Son, V. Bulovic, M. S. Dresselhaus, and J. Kong, “Large Area, Few-Layer Graphene Films on Arbitrary Substrates by Chemical Vapor Deposition,” *Nano Lett.*, vol. 9, no. 1, pp. 30–35, Jan. 2009.

[61]S. Park, K.-S. Lee, G. Bozoklu, W. Cai, S. T. Nguyen, and R. S. Ruoff, “Graphene Oxide Papers Modified by Divalent Ions—Enhancing Mechanical Properties viaChemical Cross-Linking,” *ACS Nano*, vol. 2, no. 3, pp. 572–578, Mar. 2008.

[62]S. De, P. J. King, M. Lotya, A. O'Neill, E. M. Doherty, Y. Hernandez, G. S. Duesberg, and J. N. Coleman, “Flexible, Transparent, Conducting Films of Randomly Stacked Graphene from Surfactant-Stabilized, Oxide-Free Graphene Dispersions,” *Small*, vol. 6, no. 3, pp. 458–464, Feb. 2010.

[63]S. Bae, H. Kim, Y. Lee, X. Xu, J.-S. Park, Y. Zheng, J. Balakrishnan, T. Lei, H. Ri Kim, Y. I. Song, Y.-J. Kim, K. S. Kim, B. Özyilmaz, J.-H. Ahn, B. H. Hong, and S. Iijima, “Roll-to-roll

production of 30-inch graphene films for transparent electrodes," *Nature Nanotech*, vol. 5, no. 8, pp. 574–578, Jun. 2010.

[64]C. Biswas and Y. H. Lee, "Graphene Versus Carbon Nanotubes in Electronic Devices," *Adv. Funct. Mater.*, vol. 21, no. 20, pp. 3806–3826, Sep. 2011.

[65]J. Wu, M. Agrawal, H. A. Becerril, Z. Bao, Z. Liu, Y. Chen, and P. Peumans, "Organic Light-Emitting Diodes on Solution-Processed Graphene Transparent Electrodes," *ACS Nano*, vol. 4, no. 1, pp. 43–48, Jan. 2010.

[66]M.-G. Kang, H. Joon Park, S. Hyun Ahn, and L. Jay Guo, "Transparent Cu nanowire mesh electrode on flexible substrates fabricated by transfer printing and its application in organic solar cells," *Solar Energy Materials and Solar Cells*, vol. 94, no. 6, pp. 1179–1184, Jun. 2010.

[67]L. Hu, H. S. Kim, J.-Y. Lee, P. Peumans, and Y. Cui, "Scalable Coating and Properties of Transparent, Flexible, Silver Nanowire Electrodes," *ACS Nano*, vol. 4, no. 5, pp. 2955–2963, May 2010.

[68]R. Zhu, C.-H. Chung, K. C. Cha, W. Yang, Y. B. Zheng, H. Zhou, T.-B. Song, C.-C. Chen, P. S. Weiss, G. Li, and Y. Yang, "Fused Silver Nanowires with Metal Oxide Nanoparticles and Organic Polymers for Highly Transparent Conductors," *ACS Nano*, vol. 5, no. 12, pp. 9877–9882, Dec. 2011.

[69]J.-Y. Lee, S. T. Connor, Y. Cui, and P. Peumans, "Solution-Processed Metal Nanowire Mesh Transparent Electrodes," *Nano Lett.*, vol. 8, no. 2, pp. 689–692, Feb. 2008.

[70]J. Zou, H.-L. Yip, S. K. Hau, and A. K. Y. Jen, "Metal grid/conducting polymer hybrid transparent electrode for inverted polymer solar cells," *Appl. Phys. Lett.*, vol. 96, no. 20, p. 203301, 2010.

[71]L. Hu, H. Wu, and Y. Cui, "Metal nanogrids, nanowires, and nanofibers for transparent electrodes," *MRS Bull.*, vol. 36, no. 10, pp. 760–765, Oct. 2011.

[72]D. Alemu, H.-Y. Wei, K.-C. Ho, and C.-W. Chu, "Highly conductive PEDOT:PSS electrode by simple film treatment with methanol for ITO-free polymer solar cells," *Energy Environ. Sci.*, vol. 5, no. 11, p. 9662, 2012.

[73]C.-K. Cho, W.-J. Hwang, K. Eun, S.-H. Choa, S.-I. Na, and H.-K. Kim, "Mechanical flexibility of transparent PEDOT:PSS electrodes prepared by gravure printing for flexible organic solar cells," *Solar Energy Materials and Solar Cells*, vol. 95, no. 12, pp. 3269–3275, Dec. 2011.

[74]A. G. Nasibulin, A. Kaskela, K. Mustonen, A. S. Anisimov, V. Ruiz, S. Kivistö, S. Rackauskas, M. Y. Timmermans, M. Pudas, B. Aitchison, M. Kauppinen, D. P. Brown, O. G. Okhotnikov, and E. I. Kauppinen, "Multifunctional Free-Standing Single-Walled Carbon Nanotube Films," *ACS Nano*, vol. 5, no. 4, pp. 3214–3221, Apr. 2011.

[75]Y. Zhou, L. Hu, and G. Grüner, "A method of printing carbon nanotube thin films," *Appl. Phys. Lett.*, vol. 88, no. 12, p. 123109, 2006.

[76]K. S. Kim, Y. Zhao, H. Jang, S. Y. Lee, J. M. Kim, K. S. Kim, J.-H. Ahn, P. Kim, J.-Y. Choi, and B. H. Hong, "Large-scale pattern growth of graphene films for stretchable transparent electrodes," *Nature*, vol. 457, no. 7230, pp. 706–710, Jan. 2009.

[77]X. Li, Y. Zhu, W. Cai, M. Borysiak, B. Han, D. Chen, R. D. Piner, L. Colombo, and R. S. Ruoff, "Transfer of Large-Area Graphene Films for High-Performance Transparent Conductive Electrodes," *Nano Lett.*, vol. 9, no. 12, pp. 4359–4363, Dec. 2009.

[78]C. Charton and M. Fahland, “Optical properties of thin Ag films deposited by magnetron sputtering,” *Surface and Coatings Technology*, vol. 174, pp. 181–186, 2003.

[79]A. G. Nasibulin, D. P. Brown, P. Queipo, D. Gonzalez, H. Jiang, and E. I. Kauppinen, “An essential role of CO2 and H2O during single-walled CNT synthesis from carbon monoxide,” *Chemical Physics Letters*, vol. 417, no. 1, pp. 179–184, Jan. 2006.

[80]A. G. Nasibulin, A. Ollikainen, A. S. Anisimov, D. P. Brown, P. V. Pikhitsa, S. Holopainen, J. S. Penttilä, P. Helistö, J. Ruokolainen, M. Choi, and E. I. Kauppinen, “Integration of single-walled carbon nanotubes into polymer films by thermo-compression,” *Chemical Engineering Journal*, vol. 136, no. 2, pp. 409–413, Mar. 2008.

[81]D. K. Schroder, *Semiconductor Material and Device Characterization*, 3rd ed. Wiley-IEEE Press, 2006.

[82]H. Jiang, J. Ruokolainen, N. Young, T. Oikawa, A. G. Nasibulin, A. Kirkland, and E. I. Kauppinen, “Performance and early applications of a versatile double aberration-corrected JEOL-2200FS FEG TEM/STEM at Aalto University,” *Micron*, vol. 43, no. 4, pp. 545–550, Mar. 2012.

[83]“File:Dye Sensitized Solar Cell Scheme.png - Wikimedia Commons,” *commons.wikimedia.org*. [Online]. Available: http://commons.wikimedia.org/wiki/File:Dye_Sensitized_Solar_Cell_Scheme.png.[Accessed: 21-Aug.-2013].

[84]K. Suzuki, M. Yamaguchi, M. Kumagai, and S. Yanakida, “Application of Carbon Nanotubes to Counter Electrodes of Dye-sensitized Solar Cells,” *Chemistry Letters*, vol. 32, no. 1, pp. 1–2, Feb. 2013.

[85]K. Aitola, A. Kaskela, J. Halme, V. Ruiz, A. G. Nasibulin, E. I. Kauppinen, and P. D. Lund, “Single-Walled Carbon Nanotube Thin-Film Counter Electrodes for Indium Tin Oxide-Free Plastic Dye Solar Cells,” *J. Electrochem. Soc.*, vol. 157, no. 12, p. B1831, 2010.

[86]K. Miettunen, J. Halme, M. Toivola, and P. Lund, “Initial Performance of Dye Solar Cells on Stainless Steel Substrates,” *J. Phys. Chem. C*, vol. 112, no. 10, pp. 4011–4017, Mar. 2008.

[87]M. Toivola, F. Ahlskog, and P. Lund, “Industrial sheet metals for nanocrystalline dye-sensitized solar cell structures,” *Solar Energy Materials and Solar Cells*, vol. 90, no. 17, pp. 2881–2893, Nov. 2006.

[88]J. Koskinen, J.-P. Hirvonen, and J. Keranen, “Effect of deposition temperature and growth rate on the bond structure of hydrogen free carbon films,” *J. Appl. Phys.*, vol. 84, no. 1, pp. 648–650, 1998.

[89]M. Stadermann, S. Papadakis, M. Falvo, J. Novak, E. Snow, Q. Fu, J. Liu, Y. Fridman, J. Boland, R. Superfine, and S. Washburn, “Nanoscale study of conduction through carbon nanotube networks,” *Phys. Rev. B*, vol. 69, no. 20, p. 201402, May 2004.

[90]A. S. Anisimov, A. G. Nasibulin, H. Jiang, P. Launois, J. Cambedouzou, S. D. Shandakov, and E. I. Kauppinen, “Mechanistic investigations of single-walled carbon nanotube synthesis by ferrocene vapor decomposition in carbon monoxide,” *Carbon*, vol. 48, no. 2, pp. 380–388, Feb. 2010.

[91]Y. Tian, A. G. Nasibulin, B. Aitchison, T. Nikitin, J. V. Pfaler, H. Jiang, Z. Zhu, L. Khriachtchev, D. P. Brown, and E. I. Kauppinen, “Controlled Synthesis of Single-Walled Carbon Nanotubes in an Aerosol Reactor,” *J. Phys. Chem. C*, vol. 115, no. 15, pp. 7309–7318, Apr. 2011.

[92]Y. Tian, M. Y. Timmermans, M. Partanen, A. G. Nasibulin, H. Jiang, Z. Zhu, and E. I. Kauppinen, “Growth of single-walled carbon nanotubes with controlled diameters and lengths by an aerosol method,” *Carbon*, vol. 49, no. 14, pp. 4636–4643, Nov. 2011.

[93]Z. Zhu, H. Jiang, T. Susi, A. G. Nasibulin, and E. I. Kauppinen, “The Use of NH 3to Promote the Production of Large-Diameter Single-Walled Carbon Nanotubes with a Narrow (n,m) Distribution,” *J. Am. Chem. Soc.*, vol. 133, no. 5, pp. 1224–1227, Feb. 2011.

[94]Y. Zhou, F. Zhang, K. Tvingstedt, S. Barrau, F. Li, W. Tian, and O. Inganäs, “Investigation on polymer anode design for flexible polymer solar cells,” *Appl. Phys. Lett.*, vol. 92, no. 23, p. 233308, 2008.

[95]G.-F. Wang, X.-M. Tao, and R.-X. Wang, “Flexible organic light-emitting diodes with a polymeric nanocomposite anode,” *Nanotechnology*, vol. 19, no. 14, p. 145201, Mar. 2008.

[96]H. Tantang, J. Y. Ong, C. L. Loh, X. Dong, P. Chen, Y. Chen, X. Hu, L. P. Tan, and L.-J. Li, “Using oxidation to increase the electrical conductivity of carbon nanotube electrodes,” *Carbon*, vol. 47, no. 7, pp. 1867–1870, Jun. 2009.

[97]R. Graupner, J. R. Abraham, A. Vencelov, T. Seyller, F. Hennrich, M. M. Kappes, A. Hirsch, and L. Ley, “Doping of single-walled carbon nanotube bundles by Brnsted acids,” *Phys. Chem. Chem. Phys.*, vol. 5, no. 24, p. 5472, 2003.

[98]V. Skákalová, A. B. Kaiser, U. Dettlaff-Weglikowska, K. Hrnčariková, and S. Roth, “Effect of Chemical Treatment on Electrical Conductivity, Infrared Absorption, and Raman Spectra of Single-Walled Carbon Nanotubes,” *J. Phys. Chem. B*, vol. 109, no. 15, pp. 7174–7181, Apr. 2005.

[99]B. Chandra, A. Afzali, N. Khare, M. M. El-Ashry, and G. S. Tulevski, “Stable Charge-Transfer Doping of Transparent Single-Walled Carbon Nanotube Films,” *Chem. Mater.*, vol. 22, no. 18, pp. 5179–5183, Sep. 2010.

[100]T. Minami, “Transparent conducting oxide semiconductors for transparent electrodes,” *Semicond. Sci. Technol.*, vol. 20, no. 4, pp. 35–44, Mar. 2005.

Single-walled carbon nanotube networks have a wide application potential for the future flexible and transparent electronics. This thesis focusses on the study of SWCNT networks as transparent conductive films, which can be used for a variety of applications such as touch sensors. The SWCNTs were synthesised using the aerosol-CVD process, which produces high quality SWCNTs with tunable lengths whilst membrane filtration can be used to form SWCNT-networks with tunable transparency and sheet resistance. This thesis reports significant progress in the performance of such networks, and a novel room-temperature method used to transfer the formed networks to a variety of substrates. The thesis also demonstrates several applications of such networks, including touch sensing and solar cells whilst reporting on the mechanical reinforcement of such networks by plasma-deposited carbon coatings.

Aalto-DD 197/2013

ISBN 978-952-60-5458-2
ISBN 978-952-60-5459-9 (pdf)
ISSN-L 1799-4934
ISSN 1799-4934
ISSN 1799-4942 (pdf)

Aalto University
School of Science
Department of Applied Physics

BUSINESS + ECONOMY

ART + DESIGN + ARCHITECTURE

SCIENCE + TECHNOLOGY

CROSSOVER

DOCTORAL DISSERTATIONS